Journal of Vertebrate Paleontology e1493689 (22 pages)

DOI: 10.1080/02724634.2018.1493689

ARTICLE

OSTEOHISTOLOGY OF *RAPETOSAURUS KRAUSEI* (SAUROPODA: TITANOSAURIA) FROM THE UPPER CRETACEOUS OF MADAGASCAR

KRISTINA CURRY ROGERS* and ZOE KULIK†
[1]Department of Geology, Macalester College, St. Paul, Minnesota 55015, U.S.A., rogersk@macalester.edu;

ABSTRACT—Titanosauria is a clade of sauropod dinosaurs that includes species ranging from the largest known terrestrial vertebrates to insular dwarfs no bigger than elephants. Although most sauropod dinosaurs exhibit highly vascularized fibrolamellar bone signaling rapid growth rates comparable to those of extant mammals, diminutive titanosaurs apparently exhibit histological traits consistent with reduced primary growth rates and/or truncated active growth to reach small adult body sizes. A better understanding of the evolution of titanosaur body size requires additional sampling of the 40+ known titanosaur species. The best-preserved and most complete titanosaur yet discovered is *Rapetosaurus krausei* from the Maastrichtian Maevarano Formation in Madagascar. Skeletal material from many individuals spanning a wide range of ontogeny, from neonates to very large body sizes, makes *Rapetosaurus* an ideal candidate for an analysis of growth. We analyzed *Rapetosaurus* histology using a growth series of 25 forelimb, hind limb, and girdle elements representing different ontogenetic stages, including samples from the largest *Rapetosaurus* known (femur length = 143 cm). Primary bone histology in *Rapetosaurus* is highly vascularized fibrolamellar tissue, such as is found in other sauropods and most sampled titanosaurs. Secondary remodeling begins early, as noted in other titanosaur taxa, and by mid-ontogeny is pervasive in most sampled elements. The largest known *Rapetosaurus* was still growing, whereas some small juveniles exhibit an unusual pattern of bone erosion and replacement in the context of peripheral lines of arrested growth that signal a temporary pause in bone apposition. We hypothesize that these signals may relate to the drought-stressed ecosystem inhabited by *Rapetosaurus*.

Citation for this article: Curry Rogers, K., and Z. Kulik. 2018. Osteohistology of *Rapetosaurus krausei* (Sauropoda: Titanosauria) from the Upper Cretaceous of Madagascar. Journal of Vertebrate Paleontology. DOI: 10.1080/02724634.2018.1493689.

INTRODUCTION

Titanosaurian sauropods diversified across all continents as Gondwana fragmented, and they reached a peak diversity of more than 40 known species by the end of the Cretaceous (e.g., Powell, 2003; Wilson and Upchurch, 2003; Upchurch et al., 2004; Curry Rogers, 2005; Wilson, 2005a; Gorscak and O'Connor, 2016; Paleobiology Database, 2017). Most titanosaur taxa are represented by only a few skeletal elements from a single individual, which leaves many aspects of titanosaur anatomy, ontogeny, and phylogeny poorly understood (e.g., Wilson, 2002, 2005b; Powell, 2003; Wilson and Upchurch, 2003; Upchurch et al., 2004; Curry Rogers, 2005; Salgado and Coria, 2005). Despite the limitations of their fossil record, titanosaurs exhibit an array of specializations that highlight their distinctiveness among neosauropod groups. These features include trunk and hind limb modifications that indicate a departure from the locomotor repertoire of other sauropods (Wilson and Carrano, 1999), the development of osteoderms in some species (Dodson et al., 1998; D'Emic et al., 2009; Curry Rogers et al., 2011; Lindoso et al., 2013; Salgado, 2013; Vidal et al., 2014, 2017; Carrano and D'Emic 2015; Cerda et al., 2015b; Zurriaguz, 2017), important cranial novelties (e.g., Curry Rogers and Forster, 2001, 2004; Wilson, 2005b; Wilson et al., 2016), as well as the most varied range of adult body sizes known among sauropods (e.g., Wilson and Carrano, 1999; Mazzetta et al., 2004; Curry Rogers, 2005; Stein et al., 2010; Carballido et al., 2017; Benson et al., 2018). Some titanosaur species are thought to be among the largest terrestrial vertebrates known (e.g., *Argentinosaurus*, body mass estimated at ~60,000 kg; Benson et al., 2014), whereas others are thought to have modified primary growth patterns with resultant 'dwarf' adult body sizes (*Magyarosaurus*, body mass estimated at ~750 kg; Benson et al., 2014). The life history changes that drove the wide disparity in body size remain a tenacious problem as we strive toward a better understanding of titanosaur paleobiology and evolution.

Comparative long bone histological data are available for only a small fraction of known titanosaurs. In some cases, investigators focused on long bone histology as a proxy for ontogenetic growth rates using an ontogenetic sample of multiple skeletal elements (e.g., Cerda and Powell, 2009; Klein et al., 2009, 2012; Woodward and Lehman, 2009; Stein et al., 2010; Cerda and Salgado, 2011; García et al., 2015). In other studies, the histological sample was more limited with regard to ontogeny, but these preliminary histological descriptions set the stage for ongoing deeper analysis of titanosaur growth strategies (e.g., *Saltasaurus*, Bonaparte and Powell, 1980; Cerda and Powell, 2009; Chinsamy et al., 2016; *Neuquensaurus*, Powell, 1992; Cerda and Salgado, 2011; García et al., 2015; *Mendozasaurus*, González Riga, 2003; González Riga and Curry Rogers, 2006; *Lirainosaurus*, Company, 2011; *Bonitasaura*, Gallina, 2012; *Dreadnoughtus*, Lacovara et al., 2014; *Epacthosaurus*, Cerda et al., 2015a; Brazilian

*Corresponding author.
†Current Address: Department of Biology, University of Washington, Seattle, Washington 98195-1800, U.S.A., zkulik@uw.edu
Color versions of one or more of the figures in the article can be found online at www.tandfonline.com/ujvp.

Published online 29 Oct 2018

TABLE 1. *Rapetosaurus krausei* bone histological sample.

Element	Specimen number	Length (cm)	% adult size[a]	Full (F) or partial (P) cross-section	Location of sections[b]
Humerus	UA 10011	41.1	35 (103e)	P	Lateral
	DMNH EPV.127342	63.7	63	P	Lateral
Ulna	DMNH EPV.127473	62.7	77 (81e)	P	Lateral
	DMNH EPV.127474	69.5	86	P	Lateral
Radius	DMNH EPV.127349	48.1	60 (80e)	F	Complete
Femur	DMNH EPV.127340	39.2	27 (143.4)	P	Medial
	DMNH EPV.127344	42.6	41	P	Medial
	DMNH EPV.127339	72.9	51	P	Medial
	DMNH EPV.127343	98.0	69	P	Medial
	FMNH PR 2255*	143.4	100	P	Anterior
Tibia	UA 10013	42.2	39 (109.1)	P	Anterior
	UA 10014	47.2	43	P	Anterior
	DMNH EPV.127475	57.8	53	P	Anterior
Fibula	DMNH EPV.127345	42	41 (101.7)	P	Anterior
	UA 10010	50.9	50	F	Anterior
	DMNH EPV.127346	60.6	60	P	Anterior
	DMNH EPV.127341	68.1	67	P	Anterior
Rib	FMNH PR 2209	~88	45 (>200)	F	Complete
	DMNH EPV.127350	—	50–60	P	Partial, unknown
	UA 10012	—	60–70	F	Complete
	FMNH PR 2255*	>200	100	F	Complete
Scapula	DMNH EPV.127476	36.4	32 (112.9)	P	Proximodorsal
Pubis	DMNH EPV.127348	64.4	68 (94.7)	P	Anterodorsal
Ischium	DMNH EPV.127347	40.8	79 (51.6)	P	Posterodorsal
Osteoderm	FMNH PR 2342*	57.2	100		

Specimens marked with an * are assigned to a single individual.
[a]Adult length measured or estimated ('e') by comparison to other *Rapetosaurus* associated skeletons.
[b]Sections generally extend into the mid-cortex and allowed observation of several regions of each element; e.g., a lateral section afforded views of the anterior and posterior regions.

Titanosauria indet., Ghilardi et al., 2016; *Patagotitan*, Carballido et al., 2017). Some titanosaurs are thought to continually deposit highly vascularized, fast-growing primary bone until reaching very large body sizes (e.g., *Alamosaurus*, Woodward and Lehman, 2009; Klein et al., 2012; *Bonitasaura*, Gallina, 2012; *Dreadnoughtus*, Lacovara et al., 2014; *Patagotitan*, Carballido et al., 2017), whereas other titanosaurs reveal primary bone thought to record reduced growth rates (e.g., *Phuwiangosaurus*, Klein et al., 2009; *Ampelosaurus*, Klein et al., 2012). When a downshift in bone appositional rate is combined with a truncated interval of active growth, insular dwarfism is hypothesized to result in the small-bodied *Magyarosaurus* (Stein et al., 2010) and *Lirainosaurus* (Company, 2011). Interestingly, all sampled titanosaurs exhibit an early onset of secondary remodeling (e.g., Woodward and Lehman, 2009; Stein et al., 2010; Chinsamy et al., 2016), even at neonatal ontogenetic stages (Curry Rogers et al., 2016). Moreover, many titanosaurs sampled thus far lack an 'external fundamental system' (EFS) that would indicate completion of somatic growth associated with adulthood (e.g., Klein et al., 2012; Lacovara et al., 2014; Carballido et al., 2017). In some cases (e.g., *Magyarosaurus*, Stein et al., 2010), the EFS may be obscured by extensive secondary remodeling. In other titanosaurs, secondary remodeling is less extensive, and the absence of the EFS indicates that some of the largest known sauropods were still actively growing at the time of death (e.g., Carballido et al., 2017). Notable exceptions include *Epacthosaurus* (Cerda et al., 2015a), *Saltasaurus*, and *Neuquensaurus* (Cerda and Powell, 2009; Cerda and Salgado, 2011; García et al., 2015) in which well-developed EFS indicate cessation of skeletal growth at relatively small body sizes in these taxa. The significance of these bone histological signals in relation to titanosaur growth and body size evolution requires further scrutiny, especially in species represented by a broad ontogenetic sample.

Our study focuses on the bone histology of *Rapetosaurus krausei*, a well-known titanosaur from the Upper Cretaceous Maevarano Formation of Madagascar (Curry Rogers and Forster, 2001, 2004; Curry Rogers, 2009; Curry Rogers et al., 2011, 2016). The postcranial and cranial anatomy (Curry Rogers and Forster, 2001, 2004; Curry Rogers, 2009), earliest life history (Curry Rogers et al., 2016), and paleoenvironmental context (Rogers, 2005; Rogers et al., 2007) are all documented for *Rapetosaurus*. This pre-existing context makes this taxon a prime candidate for investigating ontogenetic bone histology in a large-bodied derived titanosaur. Most importantly, the ontogenetic sample for *Rapetosaurus* is expansive and diverse and includes tiny hatchlings (femur length $\leq$20 cm), many juveniles, and large adults (femur length >140 cm) (e.g., Curry Rogers, 2009; Curry Rogers et al., 2011, 2016). Here, we employ a sample of well-preserved appendicular bones to study microstructural organization and growth patterns within and between skeletal elements throughout *Rapetosaurus* ontogeny. We relate our findings to ontogenetic growth rates and compare our results with patterns of growth hypothesized for other titanosaur taxa.

Institutional Abbreviations—DMNH EPV, Denver Museum of Nature and Science, Denver, Colorado, U.S.A.; **FMNH PR**, Field Museum of Natural History, Chicago, Illinois, U.S.A.; **UA**, Université d'Antananarivo, Antananarivo, Madagascar.

GEOLOGICAL SETTING

Fossils of *Rapetosaurus krausei* are preserved in the Maastrichtian Maevarano Formation in the central Mahajanga Basin alongside the remains of the non-avialan theropod dinosaurs *Masiakasaurus* (Sampson et al., 2001; Carrano et al., 2002; Lee and O'Connor, 2013) and *Majungasaurus* (e.g., Sampson and Krause, 2007); *Vahiny*, a second, more poorly documented titanosaurian sauropod (Curry Rogers, 2002; Curry Rogers and Imker, 2007; McNulty et al., 2010; Curry

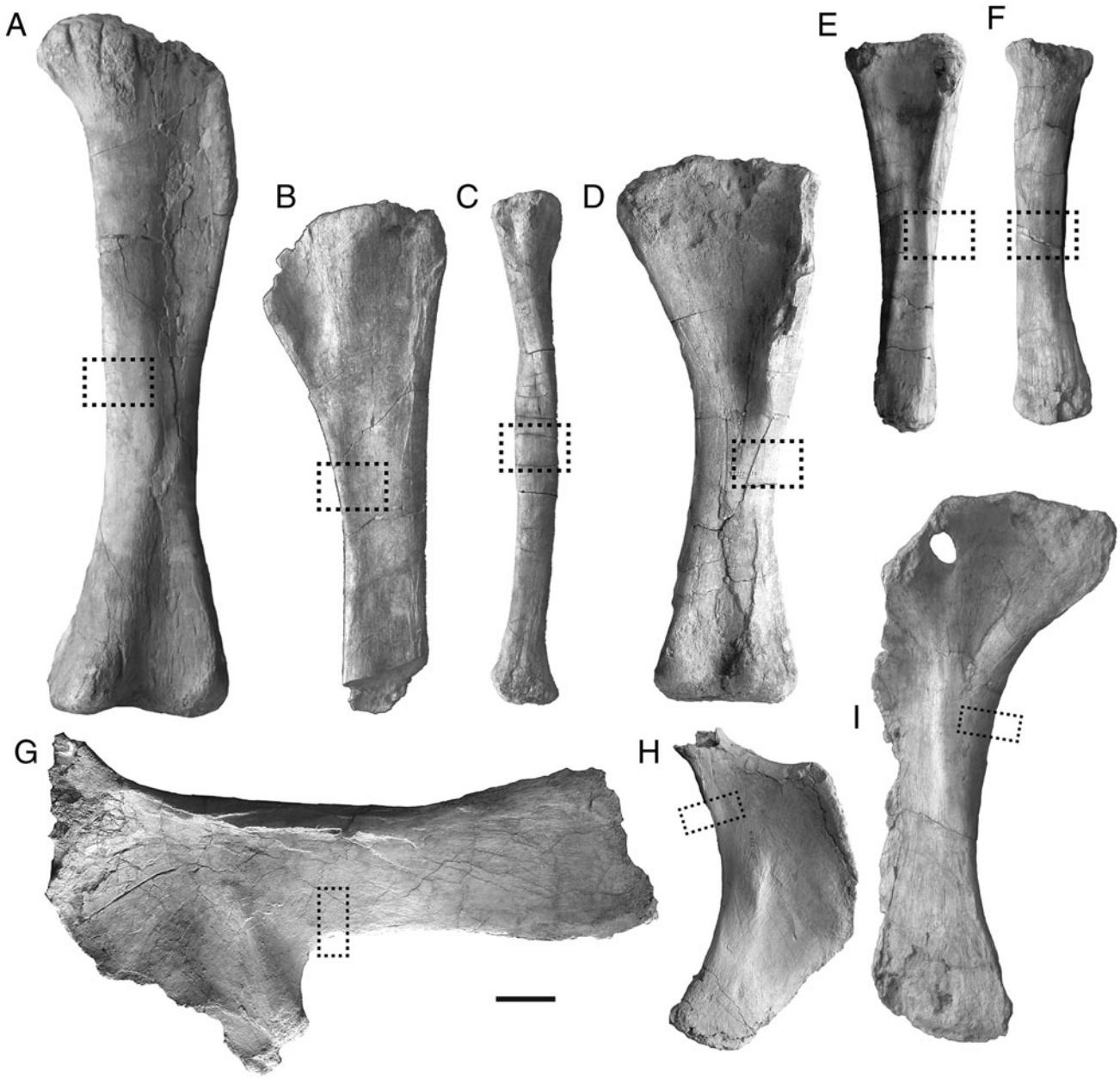

FIGURE 1. Locations of thin-sections for limb and girdle elements sampled in this study, using the well-preserved skeleton of a juvenile *Rapetosaurus krausei* (FMNH PR 2209) as an exemplar. Where possible, thin-sections extended into the deep cortex in order to capture a broad perspective on regional histology. **A**, left femur, anterior view. Femoral sections were taken from the medial surface extending into the anterior and posterior regions of the mid-diaphysis. **B**, left tibia, medial view. Tibial sections were taken from the anterior mid-diaphysis ventral to the cnemial crest and extended to medial and lateral surfaces. **C**, right fibula, anterior view. Both complete and partial sections were taken from the mid-diaphysis ventral to the lateral trochanter. Partial sections came from the anterior region of the element, extending into medial and lateral regions when possible. **D**, left humerus, anterior view. Lateral regions of the humeri were sectioned distal to the deltopectoral crest. These sections extended into the anterior and posterior regions for each element. **E**, left ulna, anterior view. Thin-sections of ulnae came from the lateral surface of each element and extended into the mid-diaphysis to include the anterior and posterior regions of the element. **F**, left radius, anterior view. A complete section of the radius came from the mid-diaphysis. **G**, right scapula, lateral view. Scapular sections came from the proximodorsal scapular blade. **H**, right ischium, lateral view. The ischium was sectioned on the posterodorsal surface, just distal to the iliac peduncle and proximal to the broad muscle scar on the lateral surface. **I**, left pubis, medial view. The pubis was sectioned from the anterodorsal surface of the proximal pubic blade, distal to the iliac peduncle. Scale bar equals 3 cm.

Rogers and Wilson, 2014); and a diversity of fish, crocodyliforms, frogs, turtles, snakes, birds, and mammals (summaries in Krause et al., 1999, 2006, 2010; Krause and Rasoamiaramanana, 2006). Sedimentological and taphonomic analyses of the sediments that preserve these fossils suggest a highly seasonal, semiarid climate that regularly stressed terrestrial vertebrates and drove mortality and preservation in the unit (Rogers et al., 2000, 2007; Rogers, 2005; Krause et al.,

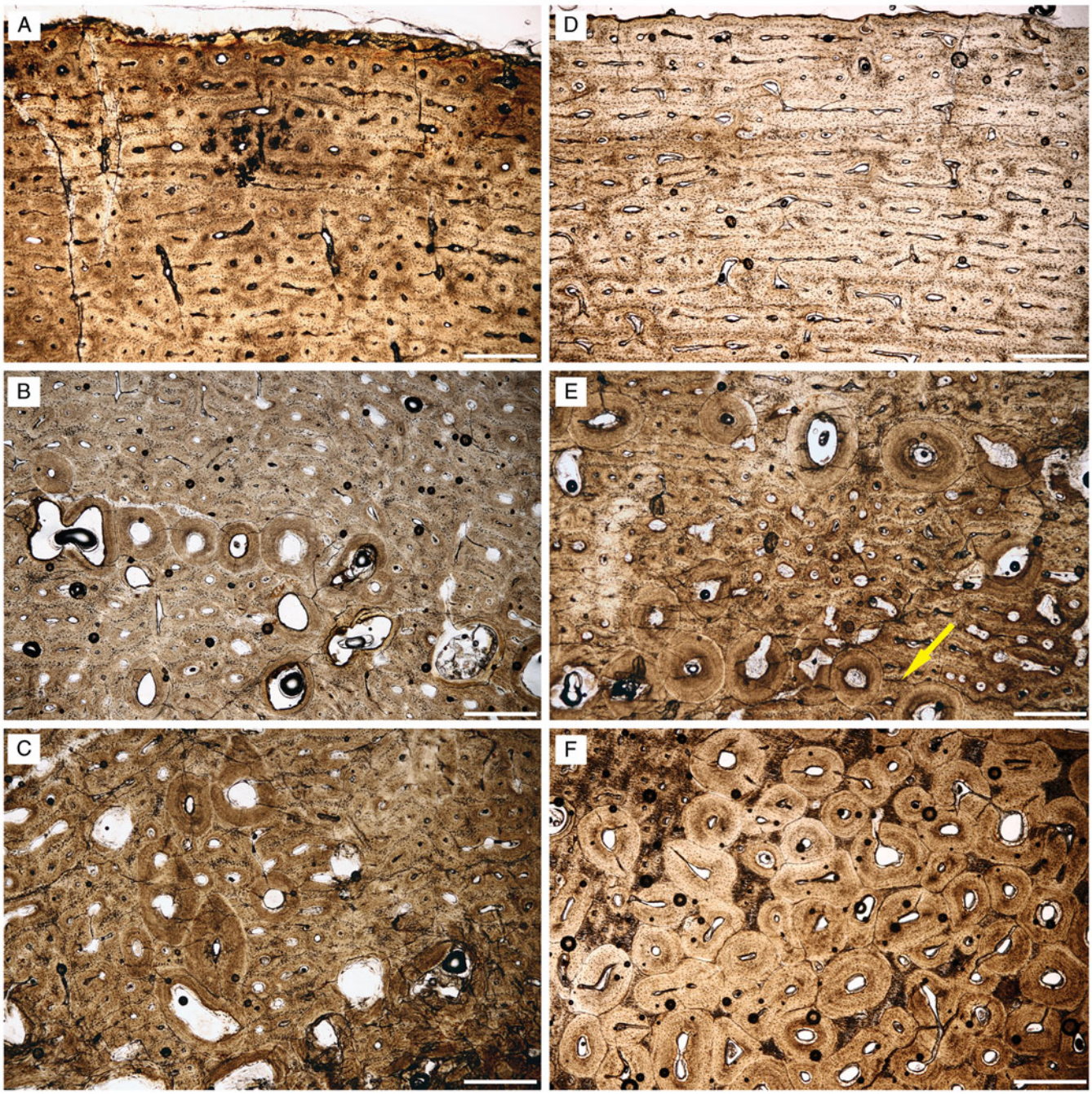

FIGURE 2. Microstructural organization of humeri in *Rapetosaurus krausei* in nonpolarized light. **A**–**C**, UA 10011 from an individual 35% adult size. **A**, fibrolamellar bone with dense longitudinal vascularity dominates the external cortex. **B**, mid-cortical circumferential bands of bone resorption. **C**, deep cortical remodeling with islands of longitudinal fibrolamellar primary bone. Some resorption cavities exceed 500 μm in diameter. **D**–**F**, DMNH EPV.127342, from an individual 63% adult size. **D**, highly vascularized longitudinal fibrolamellar bone with short circumferential anastomoses at the periosteal border. **E**, remodeling extends into the mid-cortex. A single growth mark occurs in the mid-cortex (arrow). **F**, deep cortical remodeling with small islands of primary bone and Sharpey's fibers. Scale bars equal 500 μm.

2010). Fossils of *Rapetosaurus* are common in the Maevarano Formation, with hundreds of specimens representing many individuals collected from dozens of multitaxic bonebeds since 1993 (e.g., Curry Rogers and Forster, 2001, 2004; Rogers, 2005; Curry Rogers et al., 2011, 2016).

Data suggest that there are only two titanosaur taxa present in the Maevarano Formation. *Rapetosaurus* is the better-known taxon, with an anatomical sample spanning the skeleton and skull throughout ontogeny (e.g., Curry Rogers and Forster, 2001, 2004; Curry Rogers, 2009). In contrast, *Vahiny* is currently

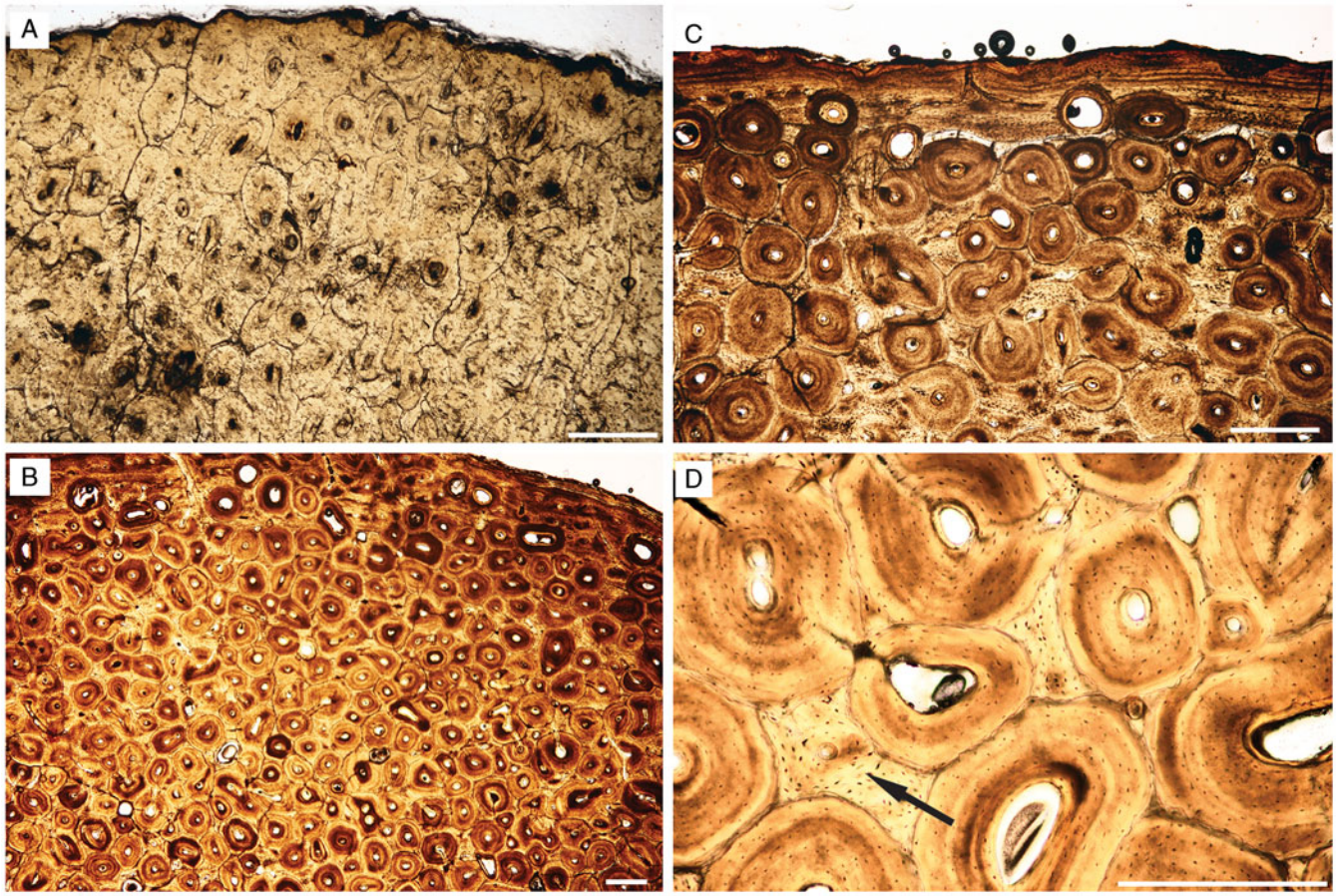

FIGURE 3. Microstructural organization of ulnae in *Rapetosaurus krausei* in nonpolarized light. **A**, DMNH EPV.127473 from an individual 77% adult size is diagenetically altered but preserves densely remodeled Haversian tissue throughout the cortex. **B–D**, DMNH EPV.127474 from an individual 86% adult size. **B**, dense remodeling extends into the outer cortex. **C**, the periosteal margin exhibits an abrupt transition in vasculature and stacked peripheral growth marks. **D**, islands of longitudinal fibrolamellar bone lacking growth marks persist in the middle and deep cortex (arrow). Scale bars equal 500 μm.

only diagnosed by cranial characters (Curry Rogers and Wilson, 2014). Rare, dissociated postcranial elements distinct from those known from *Rapetosaurus* have been recovered from the Maevarano Formation but have not yet been found in association with *Vahiny* cranial material, prohibiting the assignment of these other elements to *Vahiny* at this time (Curry Rogers and Wilson, 2014). At present, these dissociated remains are attributed to 'Malagasy Taxon B' and include caudal and sacral vertebrae, as well as elements from the forelimb and pectoral girdle from a range of body sizes that overlap with those known for *Rapetosaurus* (Curry Rogers and Imker, 2007; Curry Rogers and Wilson, 2014). The important point for this study is that we have limited our histological sampling to elements that exhibit morphological characteristics indistinguishable from those of *Rapetosaurus* specimens FMNH PR 2209 and FMNH PR 2255 (Curry Rogers and Forster, 2001, 2004; Curry Rogers, 2009; Curry Rogers et al., 2011, 2016). Additional details are available on Morphobank (Project 2724).

MATERIALS AND METHODS

Here, we add to the bone histological data reported for the smallest known *Rapetosaurus*, a tiny neonatal individual (femur length = 19 cm) described by Curry Rogers and colleagues (2016). We sampled skeletal elements that span the known size range for *Rapetosaurus*, including an array of intermediate-sized juveniles and subadults, as well as the largest known individual recovered thus far (femur length = 143 cm; FMNH PR 2255, FMNH PR 2342; Rogers et al., 2003; Curry Rogers et al., 2011).

The sample includes four ribs, one scapula, two humeri, two ulnae, one radius, one ischium, one pubis, five femora, three tibiae, and four fibulae (Table 1). A rib, femur (FMNH PR 2255), and a large osteoderm (FMNH PR 2342; Curry Rogers et al., 2011) are associated and represent a single individual as well as the largest *Rapetosaurus* specimen yet known (Curry Rogers et al., 2011). All other specimens come from several different localities within the Maevarano Formation, exhibit disparate relative sizes, and/or are ipsilateral, indicating that they each represent a single individual, for a total of 25 elements from 23 sampled individual *Rapetosaurus*. This collection of functionally disparate elements (e.g., weight-bearing limb elements vs. ribs) permits documentation of histological variation in single elements throughout ontogeny as well as in different skeletal elements from individuals of similar size/relative age.

In this study, we use the skeletal dimensions of the largest known *Rapetosaurus* specimen (FMNH PR 2255) as a reference for 'adult' size (following the approach of Woodward and Lehman, 2009). This specimen does not include an associated

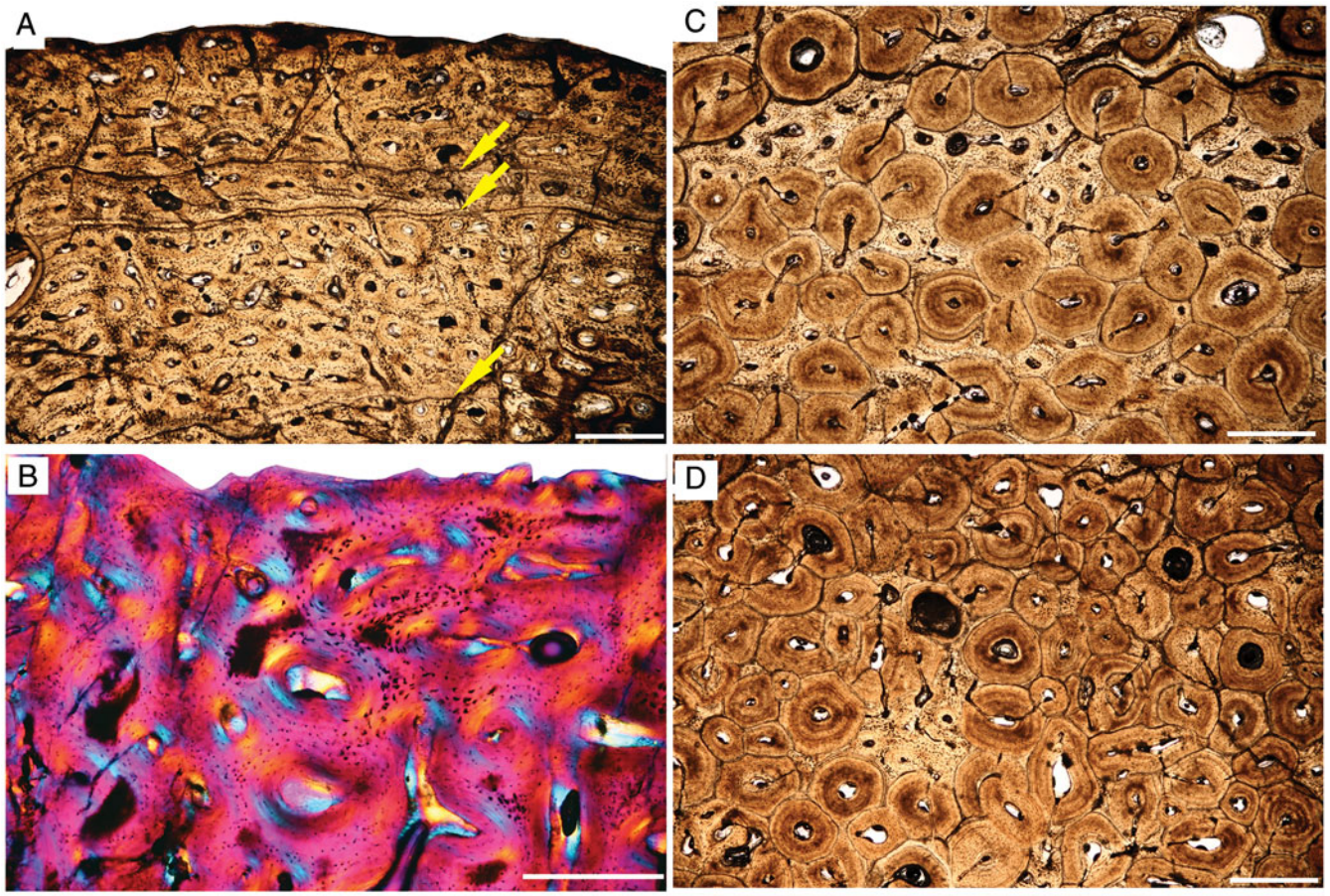

FIGURE 4. Microstructural organization of a 60% adult size *Rapetosaurus krausei* radius (DMNH EPV.127349). **A**, gross view of the external cortex in nonpolarized light, highlighting three lines of arrested growth (arrows) and densely vascularized fibrolamellar bone. **B**, longitudinally vascularized fibrolamellar primary bone at the periosteal surface in polarized light. **C**, mid-cortex in nonpolarized light, with primary fibrolamellar bone with compacted longitudinal vasculature underlying secondary osteons. **D**, growth marks are absent where primary bone persists in the middle and deep cortex. Scale bars equal 500 μm.

tibia, humerus, or fibula. For these elements, we employed ratios of limb proportions from smaller associated *Rapetosaurus* individuals along with the reported isometry of limb proportions throughout ontogeny (Curry Rogers et al., 2016) to extrapolate expected lengths at larger body size (Curry Rogers et al., 2016). In all cases, percentages of adult size should be considered estimates that allow us to discuss ontogenetic shifts in groups of bones from individuals at similar relative size (Table 1). Our assessments of relative ontogenetic stage were thus dictated primary by relative size but were also confirmed by surface texture, development/anatomy of articular surfaces, and the robustness of muscle scars and bone processes (e.g., the cnemial crest or fourth trochanter). We standardized the locations of sampling in each bone, in order to capture overlapping anatomical regions in homologous elements (Fig. 1; Table 1). Some limb elements were identified, measured, and sampled in situ during field seasons in 1999 and 2010. For these specimens, ca. 5 cm blocks were removed from mid-diaphyses or the bases of girdle element blades in the field. For specimens in museum collections, we also extracted blocks from the mid-diaphysis but only extended them through the cortex into the medullary region. These partial sections preserve element maximum length, require minimal repair, and provide a slightly expanded perspective on histological variation within samples when compared with traditional coring methods (Stein and Sander, 2009) because they can capture anterior, posterior, and medial or lateral quadrants of bone diaphyses. That said, like all methods that do not sample complete cross-sections, our window of observation is inherently limited, and entire cross-sectional histological variation within single specimens will likely be underestimated. In a few cases, our samples do span the mid-diaphyseal circumference, and this helps to contextualize expected microstructural variation for particular elements (e.g., ribs, radii, tibiae, fibulae).

Rapetosaurus bone blocks were sectioned and prepared using traditional hard-tissue sampling techniques (Lamm, 2013). We studied elements with a petrographic microscope (Nikon Eclipse 50iPOL) in plane- and cross-polarized light and obtained photomicrographs with this microscope and a Nikon DS-Fi1 digital sight camera. Composites for each thin-section were compiled with NIS-Elements BR 4.20 and are archived at MorphoBank (Project 2724). This archive includes additional montaged images of FMNH PR 2342 (Curry Rogers et al., 2011). New data presented here build upon the histological and X-ray computed tomographic (XRCT) data collected for UA 9998, the smallest known *Rapetosaurus* specimen, which has already been described in detail (Curry Rogers et al., 2016) and is also archived at MorphoBank (Project 2326). Bone histological terminology follows that of Francillon-Vieillot et al. (1990).

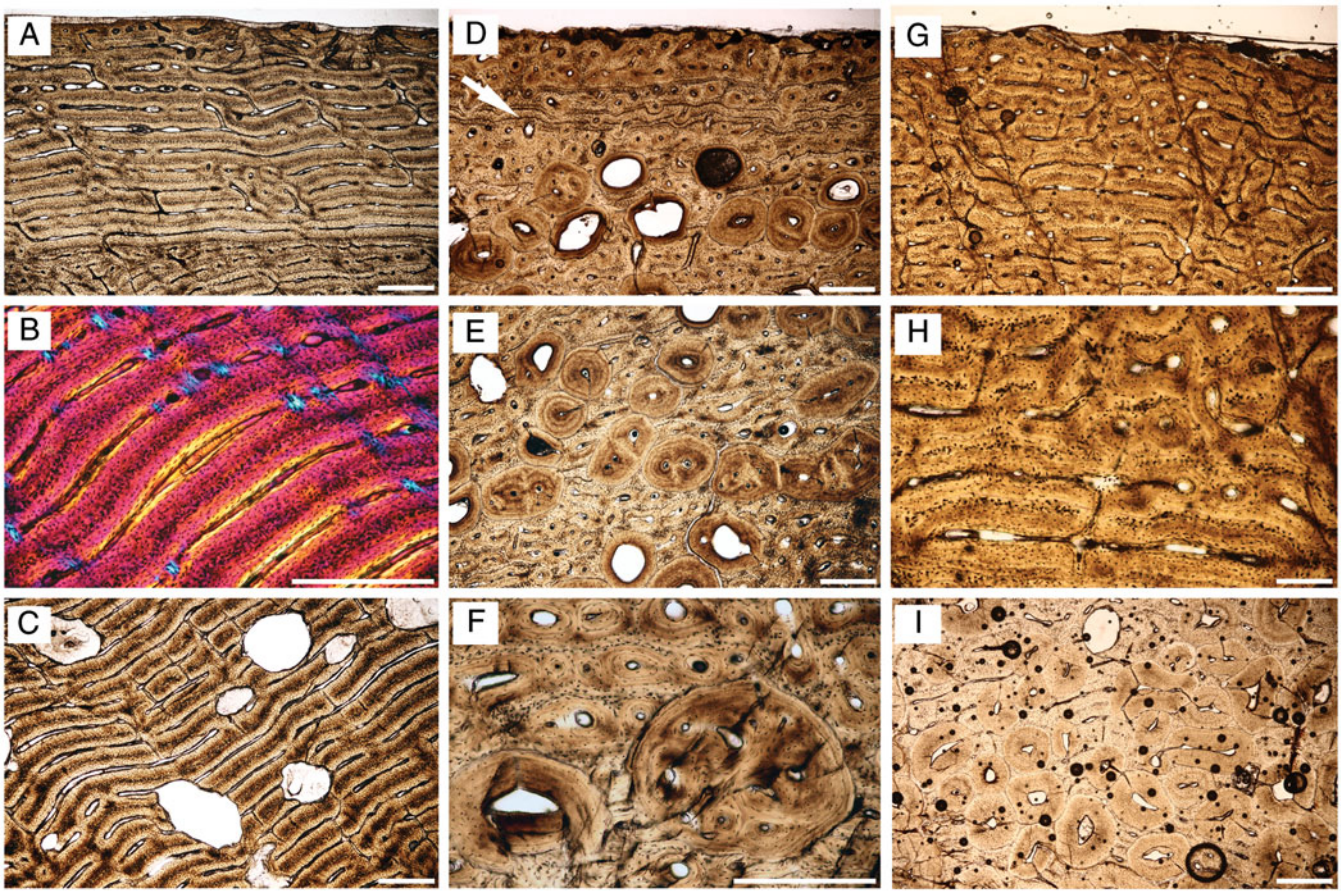

FIGURE 5. Microstructural organization of three femora in a growth series of *Rapetosaurus krausei.* All images except **B** are in nonpolarized light. **A**–**C**, DMNH EPV.127340, from an individual 27% adult size. **A**, highly vascularized, compacted laminar fibrolamellar bone in the external cortex. **B**, polarized light highlights the fibrolamellar nature of this primary bone tissue. The primary woven bone can be identified by the irregular organization of osteocyte lacunae, birefringence, and spacing between vascular canals. Later infilling of primary vascular spaces forms more highly organized primary osteons. Osteocyte lacunae are particularly dense in the woven bone component of the fibrolamellar complex. **C**, resorption cavities in this femur include some that exceed 600 μm in diameter. **D**–**F**, DMNH EPV.127344, from an individual 41% adult size. **D**, primary bone in the mid-external cortex is longitudinally vascularized. Growth marks occur near the external cortex (arrow), and some secondary osteons are organized circumferentially. **E**, remodeling extends into the mid-cortex, where abundant irregular secondary osteons are concentrated in circumferential layers. **F**, a normal (left) and an irregular (right) secondary osteon in the mid-cortex. **G**–**I**, DMNH EPV.127339, from an individual 51% adult size. **G**, primary longitudinal fibrolamellar bone lacking growth marks dominates the external cortex. **H**, primary osteons are compacted and include regions of interweaving longitudinal, circular, and occasional radial vascular canals. **I**, islands of primary bone persist in the deep and mid-cortex between secondary osteons. Scale bars equal 500 μm.

RESULTS

Bone Histology of *Rapetosaurus*

Histological descriptions are organized by skeletal element: forelimb (humerus, ulna, radius), hind limb (femur, tibia, fibula), ribs, pectoral girdle (scapula), pelvic girdle (pubis, ischium), and osteoderm. Within each bone, descriptions are organized by relative ontogenetic stage, from smallest (youngest) to largest (oldest). The largest femur and rib (FMNH PR 2255) are associated with a large osteoderm (FMNH PR 2342) described by Curry Rogers et al. (2011) and belong to a single large individual. All other sampled elements represent distinct *Rapetosaurus* individuals.

Humeri—Samples were taken from two humeri estimated at 35% and 63% adult size (Fig. 2; UA 10011, DMNH EPV.127342). In the small humerus (UA 10011), densely vascularized primary fibrolamellar bone dominates the cortex (Fig. 2A–C). The smallest canal diameters occur in the outer anterior cortex, where highly organized, infilled longitudinal primary osteons impart a distinctive 'compacted' morphology to the periosteal region of the humerus (Fig. 2A). The posterior and lateral cortices exhibit more densely vascularized primary bone. Short circumferential canals anastomose with abundant longitudinal vascular canals (Fig. 2A, C). There are no growth marks or cycles/modulations (sensu Rimblot-Baly et al., 1995; Woodward and Lehman, 2009) in the small humerus. Primary bone persists, even in the deep cortex, between a single generation of mature secondary osteons and resorption cavities (Fig. 2C). Sparse secondary osteons and large resorption cavities extend into the mid-cortex (Fig. 2B). An interesting, selective pattern of bone resorption occurs in the mid-cortex of this humerus: very large resorption cavities (>600 μm in diameter) occur in a circumferential band within a single layer, leaving unremodeled bone tissue both deeper and more superficially (Fig. 2B; Morphobank Project 2724).

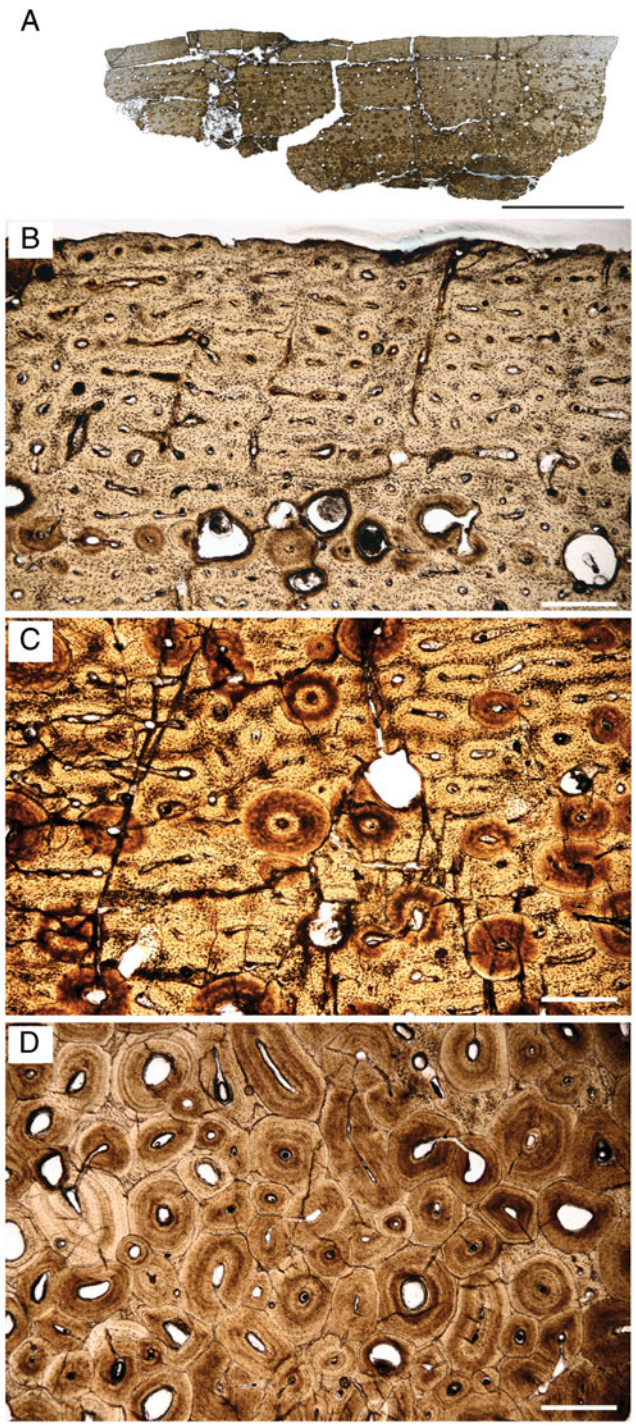

FIGURE 6. Microstructural organization of the external femoral cortex in FMNH PR 2255, the largest known individual of *Rapetosaurus krausei*, here used to represent 100% size. **A**, section taken from the anterior surface of the femoral diaphysis. **B**, the external cortex lacks LAG but retains the circumferentially focused remodeling observed in smaller femora. Fibrolamellar bone with abundant circular and longitudinal primary osteons dominates the periosteal surface. No EFS is present. **C**, remodeling extends into the mid-cortex, but persistent primary bone highlights the lack of regular growth marks in this specimen. **D**, dense Haversian bone in the deeper mid-cortex obliterates most primary bone. Scale bars equal 1 cm (**A**) and 500 μm (**B**–**D**).

The larger humerus (DMNH EPV.127342) preserves a fibrolamellar primary cortex dominated by longitudinal vascular canals connected by circumferential anastomoses (Fig. 2D, E). As in the external cortex of the smaller humerus, immature primary vascular canals are open whereas more completely infilled mature primary osteons leave only small vascular canals within centripetally deposited lamellar osteonal bone (Fig. 2D). Densely remodeled trabecular bone grades into a similarly densely remodeled deep cortex, with multiple overlapping generations of secondary osteons (Fig. 2F). Small islands of longitudinal fibrolamellar bone with occasional circular anastomoses are sometimes visible where they persist between secondary osteons in the deep cortex (Fig. 2E, F). Several mid-cortical circumferential bands of secondary bone remodeling concentrated within a single layer resemble the similar resorptive zone recorded in the smaller humerus (Fig. 2B, E). In the larger humerus, each of these bands is represented by a circumferential array of secondary osteons (Fig. 2E). The intensity of remodeling varies throughout the cross-section: the posterior aspect of the cortex exhibits a higher degree of remodeling, whereas the anterior surface exhibits a thicker external cortex of more densely vascularized primary fibrolamellar bone. A single growth mark present in the mid-cortex is overprinted by a single generation of secondary osteons (Fig. 2E).

Ulnae—Two ulnae were sampled: one at 77% adult size and one at 86% adult size (Fig. 3; DMNH EPV.127473, DMNH EPV.127474). Bone histology in the smaller ulna is not particularly well preserved (DMNH EPV.127473; Fig. 3A), but where visible, a thick primary cortex has been intensely remodeled by multiple generations of secondary osteons to form dense Haversian bone (Francillon–Vieillot et al., 1990). The periosteal border of this specimen is avascular and smooth (Fig. 3A).

A second, slightly larger ulna (DMNH EPV.127474; Fig. 3B–D) preserves small pockets of longitudinal fibrolamellar primary bone between multiple generations of mature, secondary osteons in the mid-cortex. The periosteal primary bone shifts abruptly from longitudinally vascularized fibrolamellar bone to avascular, lamellar, and parallel-fibered tissue (Fig. 3C). Growth marks are absent in the mid-cortex where primary bone is preserved (Fig. 3C, D). Stacked growth marks that cannot be traced circumferentially but approximate the EFS are preserved in zones of the periosteal surface (Fig. 3B, C). Remodeling in this ulna is pervasive, especially in the deep cortex (Fig. 3D), and extends into regions of the outermost cortex, obliterating most evidence of primary bone deposition (Fig. 3B, C).

Radius—A 60% adult size radius retains primary bone in small zones, even within the deep cortex (Fig. 4; DMNH EPV.127349). Longitudinal and longitudinal-reticular fibrolamellar bone exhibits narrow vascular spaces infilled by centripetal bone deposition that diminishes primary porosity in the deep and mid-cortex (Fig. 4A, B). In the external cortex, several irregularly spaced growth marks punctuate more prevalent longitudinal primary fibrolamellar bone (Fig. 4A). The deepest growth mark is a single annulus with a crack formed along it that is impossible to trace circumferentially. A line of arrested growth (LAG) preceded by a wide zone of longitudinally vascularized primary fibrolamellar bone with occasional radial anastomoses constitutes the second growth mark (Fig. 4A). The third and most external growth mark closely follows this LAG, with only a single layer of mostly longitudinal fibrolamellar bone between the second and third growth marks (Fig. 4A). More highly vascularized longitudinal fibrolamellar bone deposition resumes after this third pause in appositional growth and continues unabated to the periosteal margin of the radius (Fig. 4A, B). A robust lamellar infill surrounding

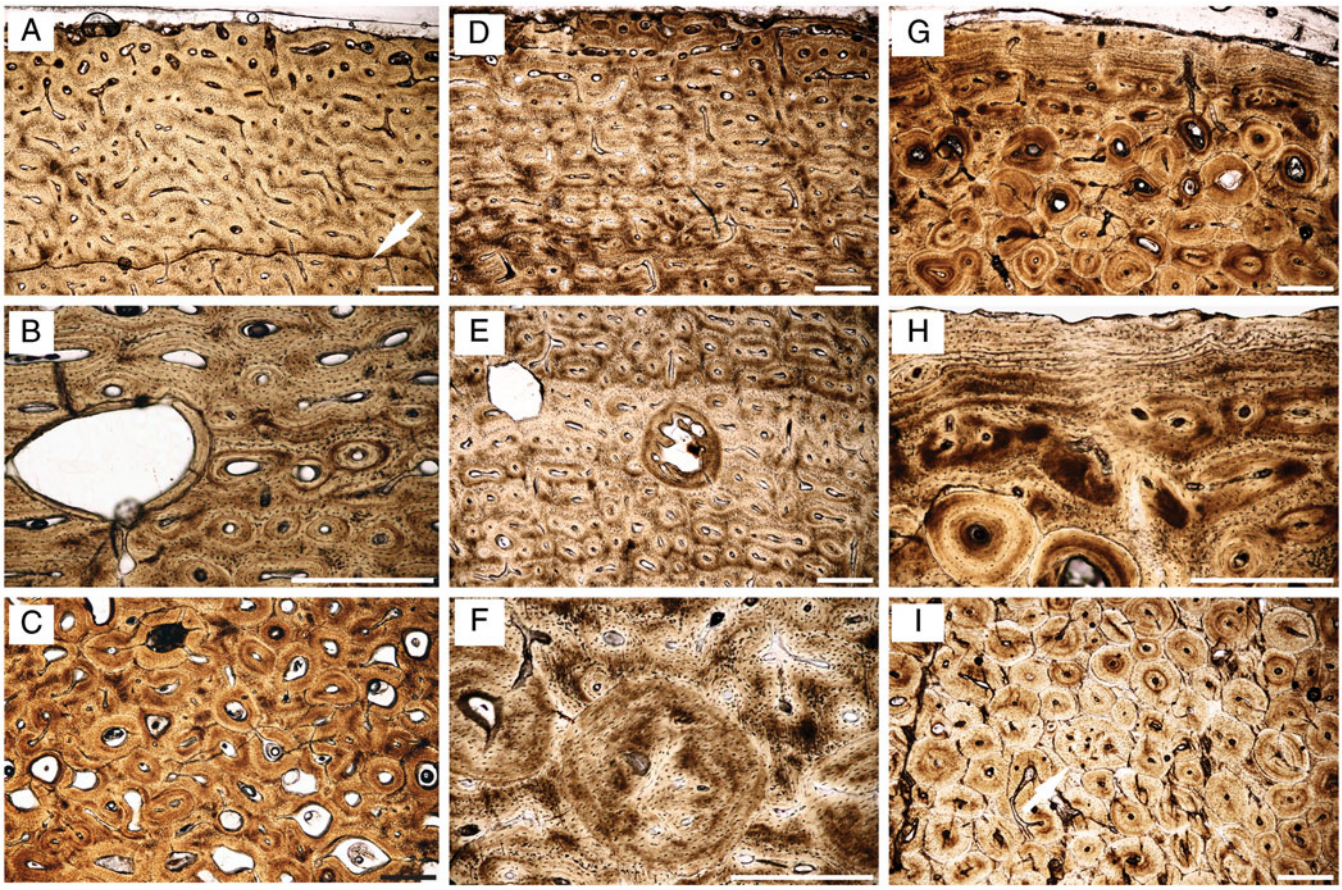

FIGURE 7. Microstructural organization of three tibiae in a growth series of *Rapetosaurus krausei* in nonpolarized light. **A**–**C**, UA 10013 from an individual 39% adult size. **A**, highly vascularized longitudinal fibrolamellar bone in the external cortex exhibits a single LAG (arrow) that cannot be traced circumferentially. **B**, resorption cavities in the mid-cortex are often focused on a single circumferential layer and can exceed 600 μm in diameter. **C**, the deep cortex has undergone significant remodeling and lacks irregular osteons. **D**–**F**, UA 10014, from an individual 43% adult size. **D**, longitudinally vascularized fibrolamellar bone with occasional radial and circular anastomoses dominates the external cortex. **E**, an irregular osteon captured during centripetal deposition following intense resorption of a large cavity. **F**, a normal (right) and an irregular (left) secondary osteon in the mid-cortex with primary bone, including abundant Sharpey's fibers. **G**–**I**, DMNH EPV.127475, from an individual 53% adult size. **G**, the external cortex transitions abruptly from longitudinal and circular primary osteons to stacked avascularized lamellae similar to the EFS. **H**, remodeling extends into the external cortex, with avascular lamellae at the periosteal surface. **I**, dense Haversian bone in the deeper mid-cortex obscures most primary bone. A few irregular osteons also persist in the mid-cortex. Scale bars equal 500 μm.

primary vascular spaces imparts a compacted morphology to the cortex (Fig. 4A–C). Resorption cavities and a single generation of secondary osteons are present in the mid-cortex (Fig. 4C, D). The radius exhibits at least two generations of secondary osteons in the deep cortex, obliterating most primary bone tissue (Fig. 4D).

Femora—We sampled five femora ranging from 27% to 100% adult size (Figs. 5, 6; Table 1). One of these femora (DMNH EPV.127343) is too poorly preserved to figure here but is included in the MorphoBank archive (Project 2724).

The spongiosa is not preserved in the smallest femur (DMNH EPV.127340), but the young cortex is characterized by primary fibrolamellar bone with numerous circular, longitudinal, and rare radial vascular canals constituting a mostly laminar primary vascular network (Fig. 5A–C). The primary vascular spaces tend to be intensely infilled, which at first pass indicates that the element is dominated by lamellar bone. The robust infilling of primary osteons imparts the same 'compacted' morphology to primary bone tissue observed in other elements. Osteocyte lacunae are so densely packed within the woven scaffold of the fibrolamellar complex that they can easily be mistaken in gross views for mineralized growth marks (Fig. 5A, C), but growth marks are absent in this small femur. Secondary osteons are also absent. A single generation of bone resorption has left broad, large (>600 μm in diameter) resorption cavities throughout the cortex (Fig. 5C). These resorption cavities are largest deeper in the cortex and diminish in size toward the periosteal margin of the element.

A femur from an individual of ca. 41% adult size (DMNH EPV.127344) exhibits a thick cortex of longitudinal fibrolamellar primary bone tissue similar to the 'compacted' microstructure described for other elements (Fig. 5D–F). Externally, densely vascularized primary, longitudinal fibrolamellar bone exhibits fewer circular anastomoses (Fig. 5D). Cortical growth marks are present in this femur (Fig. 5D). The outermost cortex records a transition to slower-growing lamellar bone with stacked growth lines (Fig. 5D, E). At least two generations of secondary osteons obliterate most primary bone in the deeper

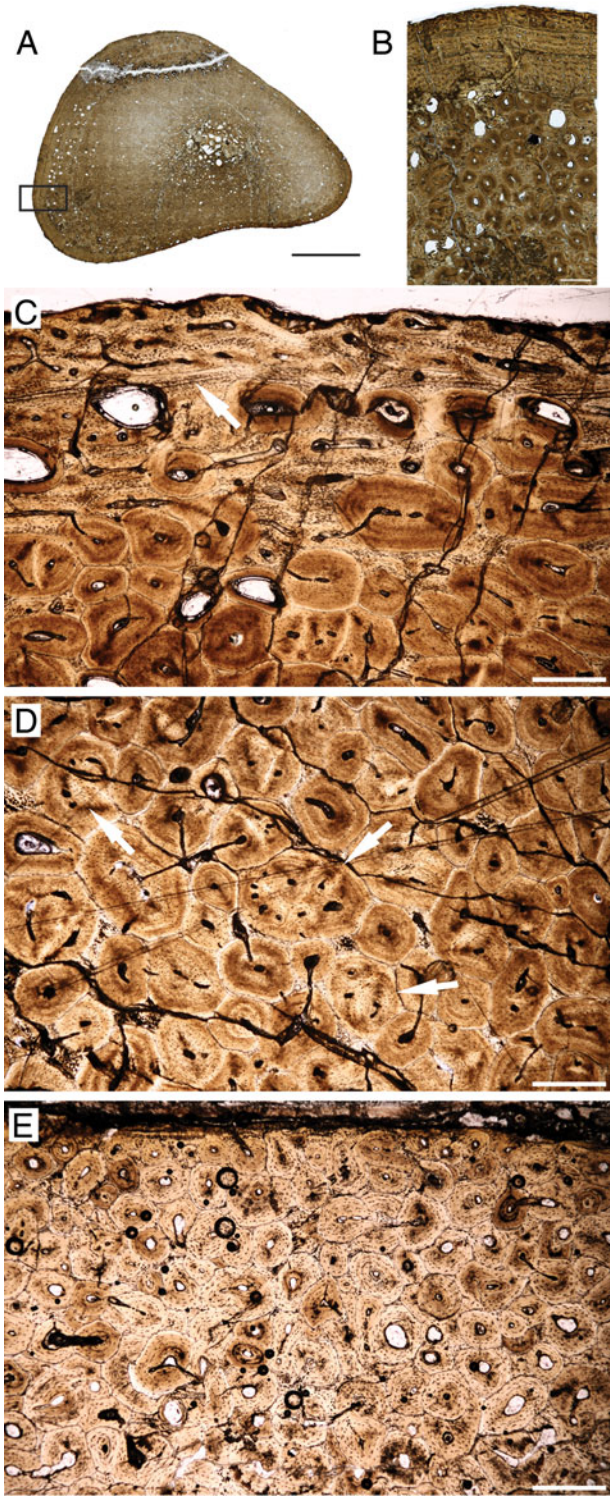

FIGURE 8. Microstructural organization of fibulae in a growth series of *Rapetosaurus krausei* in nonpolarized light. **A–D**, DMNH EPV.127345, from an individual 41% adult size. **A**, gross view of the fibula cross-section highlights remodeling that extends into the mid-cortex. Primary bone at the external cortex (box) is highlighted in B and C. **B**, longitudinal fibrolamellar bone at the periosteal surface exhibits several growth marks. **C**, highly vascularized fibrolamellar bone in the external cortex is punctuated by stacked LAG (arrow). **D**, irregular secondary osteons (arrows) alongside normal secondary osteons in the mid- and deep cortex. **E**, all other sampled fibulae (UA 10010, 50%; DMNH EPV.127346, 60%; and DMNH EPV.127341, 67% adult size) exhibit complete remodeled cortices. This pattern is illustrated here in UA 10010, from an individual ca. 50% adult size. Scale bars equal 1 cm (**A**) and 500 μm (**B–E**).

cortex, and sparse secondary remodeling extends into the mid-cortex. Secondary osteons and resorption cavities are sometimes aligned in a single circumferential layer within a layer (Fig. 5D, E). Two types of secondary osteons occur in this femur. Most are normal, ranging in diameter from ca. 150 to 350 μm, and most exhibit a single, central vascular canal (Fig. 5E, F). Other secondary osteons are unusually large, with circumferences as much as four times larger than typical osteons (Fig. 5F). These osteons capture multiple vascular bundles and are distinctive from a simple coalescence of multiple smaller secondary osteons because all Haversian canals are captured within a single external cementing line. For these osteons, the first pulse of centripetal infill takes the form of a circumferential layer of highly organized lamellar bone lacking abundant osteocyte lacunae. This nearly acellular 20–30 μm zone grades into centripetal deposits of more typical lamellar bone tissue, with organized osteocyte lacunae surrounding vascular canals (Fig. 5F). For all remaining descriptions, secondary osteons with this suite of unusual characteristics will be described as 'irregular osteons.' Irregular osteons occur throughout the cortex of this juvenile femur, but in some areas they are circumferentially arranged along a single layer of primary fibrolamellar bone (Fig. 5E, F). The large resorption cavities observed in the smallest femur (27% adult size; Fig. 5C) potentially presage the formation of irregular osteons.

The primary cortical bone in a 51% adult size femur (DMNH EPV.127339) exhibits longitudinal fibrolamellar primary bone with occasional interweaving circular and radial canals (Fig. 5G–I). Primary vascular canals are compacted like those documented in smaller femora, and intercalated deposits of woven bone in the outer cortex contain abundant osteocyte lacunae (Fig. 5G, H). Patchy remnants of primary bone are visible even in the deeper regions of the cortex, which have been intensely remodeled (Fig. 5I). The deep cortex is crushed but exhibits closely spaced overlapping secondary osteons. Remodeling extends into the mid-cortex, where it is less dense and less extensive than in smaller femora (e.g., DMNH EPV.127344). Irregular osteons do not occur in this element, although some secondary osteons with single vascular canals do exhibit relatively large diameters (~600 μm; Fig. 5I).

Remodeling, diagenesis, and crushing obscure most details of primary bone histology in a femur from an individual of 69% adult size (DMNH EPV.127343), so it is not figured here (Morphobank Project 2724). As in other elements, centripetal lamellar bone deposition within primary vascular spaces compacts primary osteons. Most externally, the primary bone is highly organized and shifts to a more parallel-fibered organization with small-diameter longitudinal primary canals. A crack in the outer cortex may follow a peripheral LAG and marks a transition between more highly vascularized fibrolamellar bone and more organized primary tissue externally. In some regions of the cross-section, the periosteal border is avascular, but peripheral LAG constituting an EFS are absent. Remodeling is pervasive throughout this femoral cross-section, with dense Haversian bone extending into the external cortex, leaving only a thin rim of primary bone at the periosteal surface. Irregular secondary osteons are absent.

The largest sampled femur comes from the largest known *Rapetosaurus* individual and is thus interpreted to represent 100% of adult size in our sample (FMNH PR 2255; Fig. 6). This femur is directly associated with the largest rib (described below) and a large osteoderm (FMNH PR 2342; Curry Rogers et al., 2011). Our sample was taken from the anterior surface and, because of the large size of the element, extended only into the mid-cortex (Fig. 6A). Primary bone microstructure is consistent throughout the cross-section, with longitudinal primary osteons vascularizing a woven bone scaffold that is rich

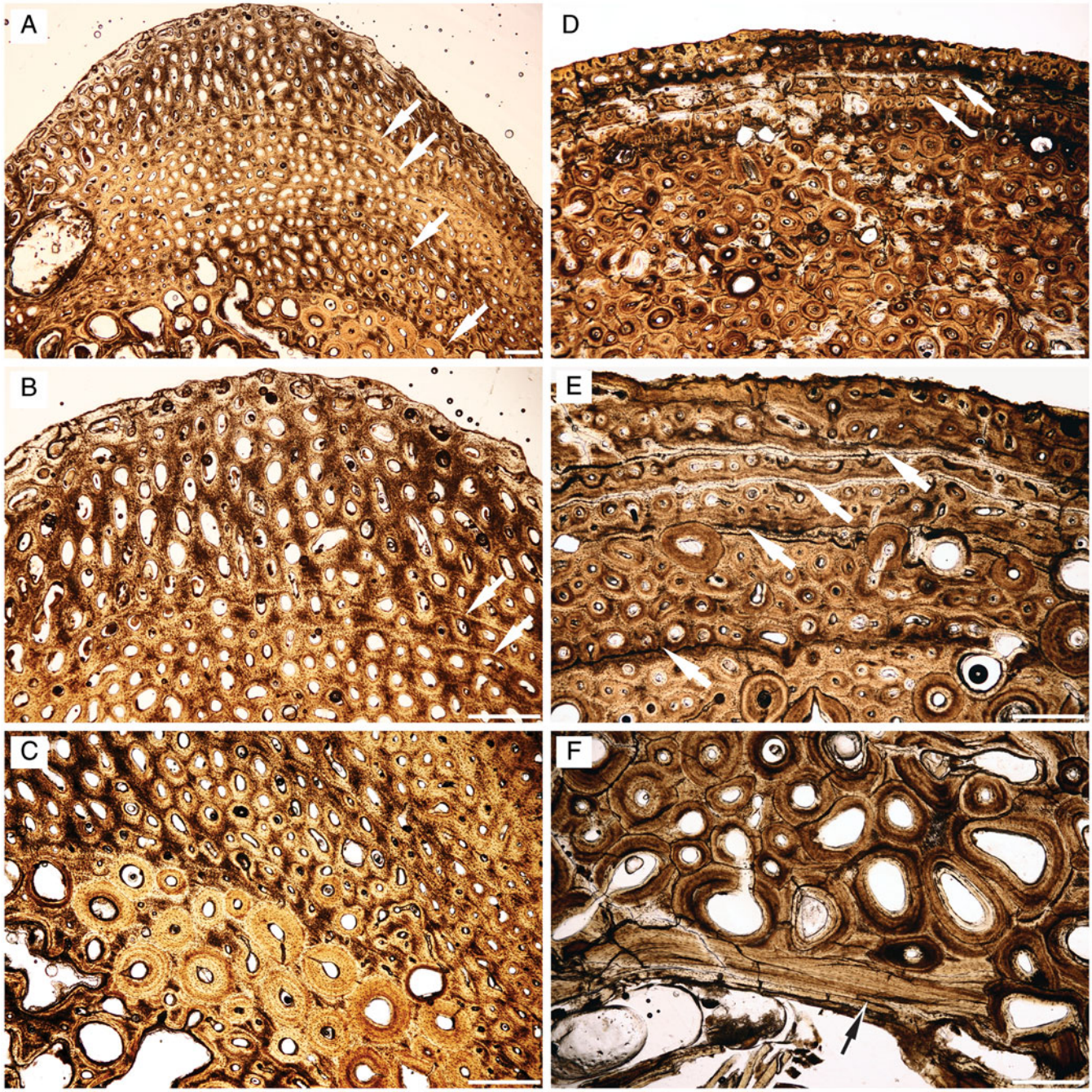

FIGURE 9. Microstructural organization of ribs in a growth series of *Rapetosaurus krausei* in nonpolarized light. **A**–**C**, FMNH PR 2209, from an individual 45% adult size. **A**, highly vascularized, fibrolamellar bone in the external cortex is punctuated by irregularly spaced growth marks that are difficult to trace circumferentially (arrows). **B**, densely packed osteocyte lacunae dominate the woven component of the fibrolamellar complex. Growth marks in this element include irregularly spaced LAG and annuli (arrows). **C**, deep cortex records remodeling a single generation of secondary osteons and primary bone dominated by longitudinal vascular canals. Delicate fibers associated with the secondary trabecular bone and secondary endosteal bone (bottom left) are consistent with pneumaticity. **D**–**F**, FMNH PR 2255, from the largest sampled *Rapetosaurus* individual, here representing adult size. Other sampled ribs (DMNH EPV.127350, 50–60% adult size; UA 10012, 60–70% adult size) illustrate similar patterns of bone deposition (Morphobank Project 2724). **D**, in larger ribs such as FMNH PR 2255, growth cycles are more prevalent and are demarcated by LAG that can be traced circumferentially. Remodeling extends into the mid cortex (arrows). **E**, primary bone includes deeper and mid-cortical fibrolamellar tissue that grades externally into more organized lamellar-fibered primary bone. Circumferential LAG punctuate primary bone deposition in the mid-cortex (arrows). **F**, endosteal bone lining pneumatic cavity grades into densely remodeled trabecular bone (arrow). Scale bars equal 500 μm.

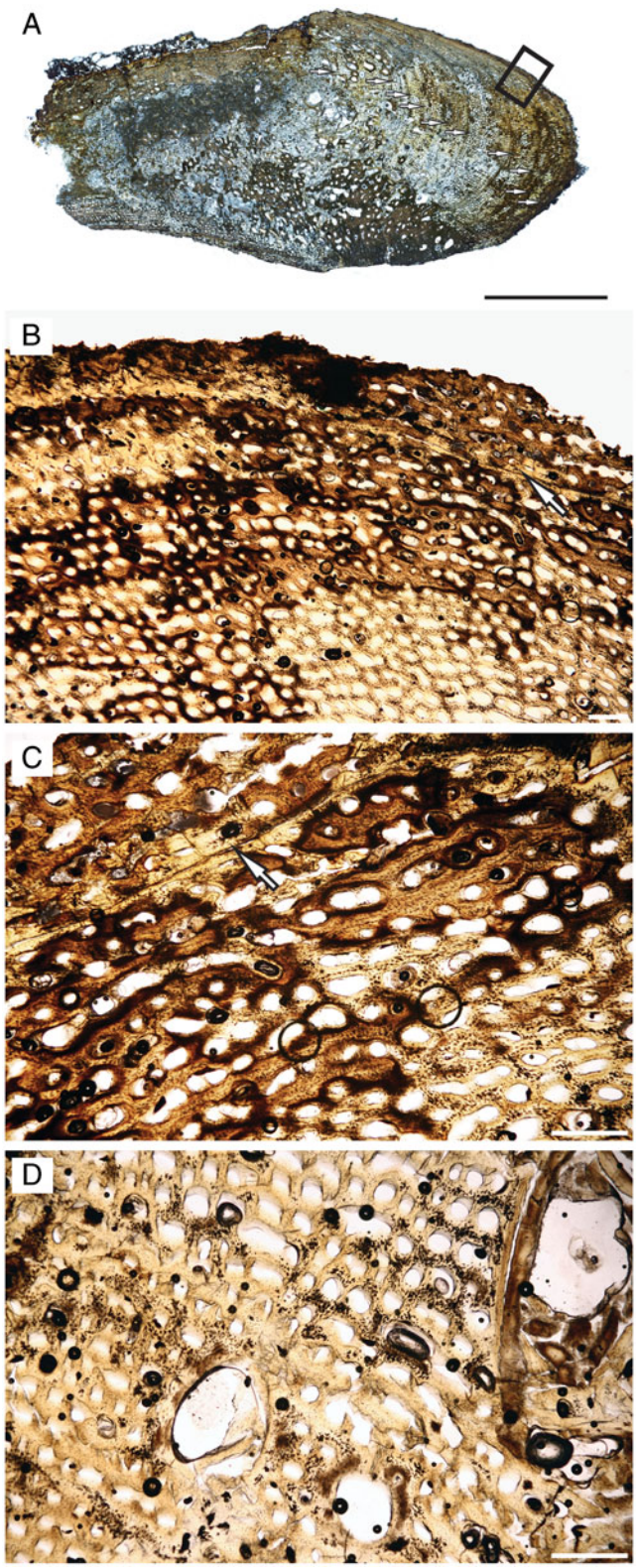

FIGURE 10. Microstructural organization of a 32% adult size *Rapetosaurus krausei* scapula (DMNH EPV.127476). **A**, a gross view of the scapula section in nonpolarized light, highlighting cyclical patterns of primary bone deposition (arrows). Box indicates position of **B**. **B**, some cycles are bound by LAG (arrow), whereas others are demarcated by a subtle shift in vascular organization. **C**, close-up view of LAG shown in **B**. **D**, large resorption cavities extend into the mid-cortex and primary bone is densely vascularized with longitudinal vascular canals. Scale bars equal 1 cm (**A**) and 500 μm (**B**–**D**).

with osteocyte lacunae (Fig. 6B, C). No LAG or other growth marks are present in this element, even at the outer cortex, although in some cases a dense layer of osteocyte lacunae easily can be mistaken for a LAG in gross view (Fig. 6B). Immature, open primary longitudinal vascular canals line the periosteal border and indicate that growth is ongoing, even in this very large individual (Fig. 6A). Irregular osteons are also absent within the preserved cortex, although a single generation of normal secondary osteons extends toward the external cortex (Fig. 6C, D). Interestingly, although this thin-section comes from the anterior mid-diaphysis of a femur that is 143 cm long, histology is consistent with a lower 'histologic ontogenetic stage' (HOS; Klein and Sander, 2008) than that documented for a smaller juvenile femur (the specimen representing 41% adult size; Fig. 5D–F).

Tibiae—Mid-diaphyseal sections were made for three tibiae ranging in size from 39% to 53% adult size (Fig. 7; Table 1). The smallest tibia (UA 10013; Fig. 7A–C) is dominated by longitudinal fibrolamellar primary bone throughout the cortex (Fig. 7A, B). Osteocyte lacunae are densely packed within the woven component of the fibrolamellar complex, and primary osteons are densely infilled. Occasional circular and radial anastomoses impart a 'subplexiform and/or sublaminar' vascular pattern in some regions of the mid-cortex (Fig. 7A). A single growth mark in the outer third of the cortex cannot be traced throughout the cross-section, but it occurs within the context of highly vascularized fibrolamellar bone where visible (Fig. 7A). Most externally, this tibia exhibits open primary vascular canals that signal ongoing appositional growth (Fig. 7A). A single generation of bone remodeling results in well-developed perimedullar secondary osteons (Fig. 7C). Resorption cavities and sparse secondary osteons extend into the mid-cortex. As in the smallest sampled humerus and femur, a single cycle of bone remodeling is underway in the mid-cortex, with broad, open resorption cavities exceeding 600 μm in diameter (Fig. 7B). Also similar to the other small sampled appendicular elements, mid-cortical bone remodeling is sometimes focused within circumferential bands in single layers, leaving unremodeled bone tissue both deeper and more superficially. This tibia lacks irregular secondary osteons (Fig. 7C).

A 43% adult size tibia (UA 10014; Fig. 7D–F) preserves a thick cortex constituted by primary fibrolamellar bone. In the deep cortex, longitudinal primary bone with occasional radial and circular anastomoses predominates. In the mid-cortex, longitudinal primary osteons are more common, with fewer occasional circular and radial anastomoses (Fig. 7E). Throughout the element, primary vascular canals are highly infilled with circumferential lamellae, which results in a significant narrowing of primary vascular space following an initial pulse of woven bone deposition. Active growth at the periosteal surface is indicated by the scalloped margins of open vascular spaces (Fig. 7D). Sharpey's fibers are abundant in the anterior cortex (Fig. 7F). The deepest cortex is extensively remodeled with multiple, overlapping generations of secondary osteons that obliterate most signals of primary growth (Fig. 7F). Secondary remodeling extends into the mid-cortex, with some resorption cavities and immature secondary osteons arranged in circumferential rows. Irregular osteons are present within the deep and middle cortex, where they capture up to eight vascular canals (Fig. 7E, F).

The deep-middle cortex of a tibia that is interpreted to represent 53% adult size (DMNH EPV.127475; Fig. 7G–I) records sparse pockets of fibrolamellar primary bone tissue characterized by abundant but densely infilled and compacted longitudinal primary osteons (Fig. 7G–I). The cortex maintains this trend with abundant and mostly infilled primary longitudinal vascular canals that transition sharply at the periosteal surface

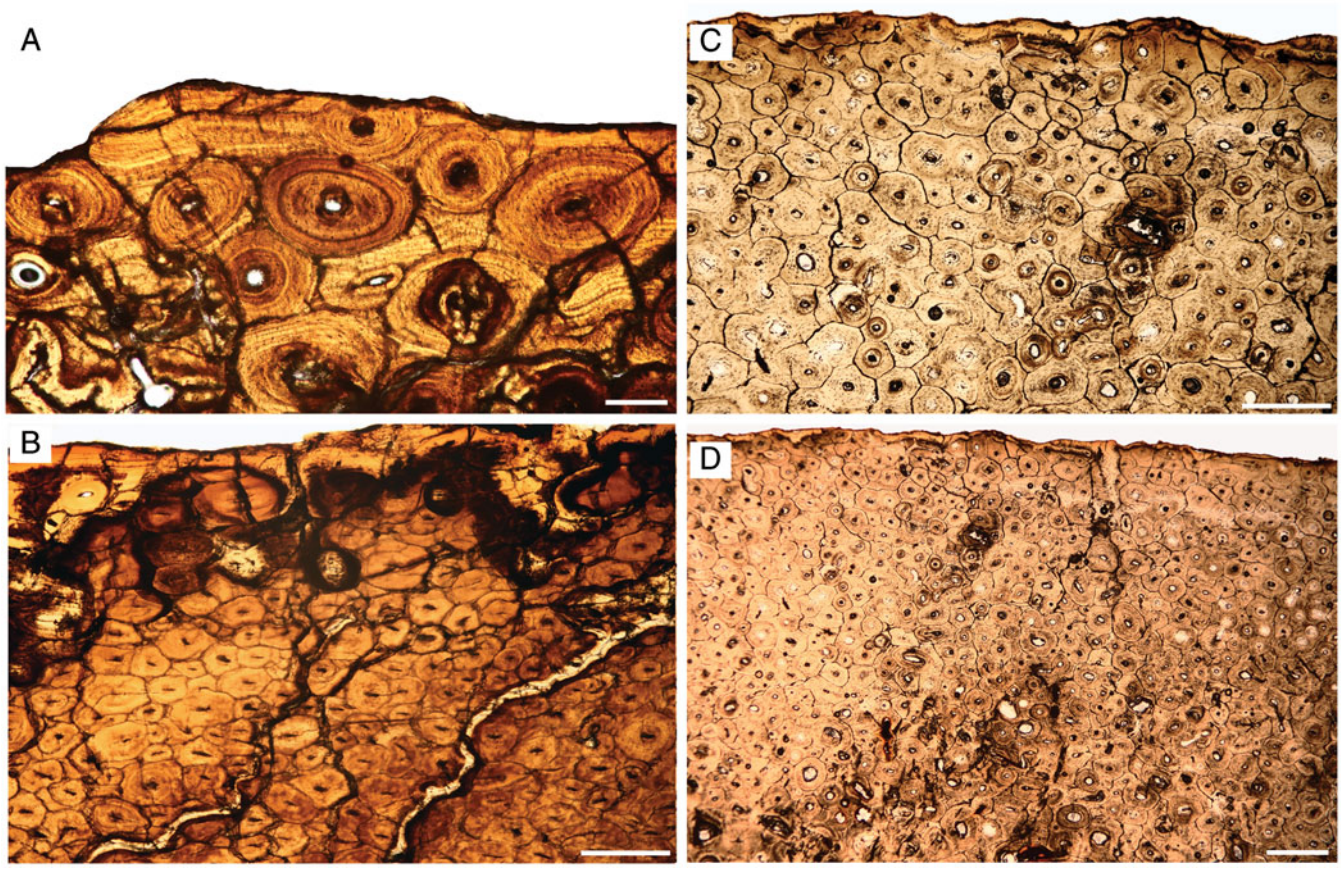

FIGURE 11. Microstructural organization of pelvic girdle elements in *Rapetosaurus krausei.* **A**, **B**, DMNH EPV.127348, a pubis 68% adult size. **A**, primary bone is visible only at the periosteal surface, where it is lamellar-fibered and avascularized. **B**, the cortex of the pubis is densely remodeled. **C**, **D**, DMNH EPV.127347, an ischium 79% adult size shares general organization with the pubis. **C**, remodeling obscures primary bone signal except at the periosteal border of the lateral surface of the element. A very thin layer of avascular lamellar primary bone characterizes the periosteal margin. **D**, the ischium is densely remodeled on the medial surface of the element as well, with only a thin rim of primary bone visible at the periosteal surface. Scale bars equal 500 μm.

to a zone of avascularized lamellar bone with stacked lamellae that resemble the EFS (Fig. 7G, H). In some regions of the outer cortex, a zone of longitudinal fibrolamellar bone apposition follows these lamellae (Fig. 7G). Several generations of remodeling in the deeper cortex result in perimedullar dense Haversian bone (Fig. 7I). Throughout the element, secondary osteons and resorption cavities are normal and only a few irregular osteons occur in the mid-cortex (Fig. 7I).

Fibulae—Our sample includes four fibulae spanning 41–67% adult size (Table 1). The smallest sampled fibula is the only specimen to retain a primary bone signal (Fig. 8A–D; DMNH EPV.127345). This primary organization is visible in scattered patches of the cortex between areas of dense secondary remodeling, in the mid-cortex, and at the periosteal surface (Fig. 8A–D). Longitudinal fibrolamellar bone tissue dominates the primary cortex (Fig. 8A–C). A multiple-LAG annulus occurs in avascularized, lamellar primary bone at the element's medial periosteal border (Fig. 8C). These stacked LAG are followed by renewed deposition of longitudinally vascularized primary bone (Fig. 8A–C). In other areas of the external cortex, these LAG can be traced deeper to the periosteal surface, where they are followed by the deposition of fibrolamellar bone tissue with immature longitudinal primary osteons (Fig. 8B) at the element's periosteal border. In spite of the small relative size of this element, dense Haversian bone is abundant, and this tissue overprints most of the primary signal in the deep and middle cortex, with secondary osteons extending to the external cortex throughout the cross-section (Fig. 8A, C, D). Both normal and irregular osteons are present in this specimen. Irregular osteon diameters are 840 μm on average (n = 15) (Fig. 8D).

All other sampled fibulae (50%, 60%, and 67% adult size, respectively) are characterized by the same basic bone histological patterns (Fig. 8E; Morphobank Project 2724). We illustrate these patterns in UA 10010 (Fig. 8E; Morphobank Project 2724). In these bones, primary bone tissue is only visible as small islands in the external cortex and primary longitudinal fibrolamellar bone is common (Fig. 8E). The periosteal cortices of all three elements exhibit thin layers of sparsely longitudinally vascularized or avascular lamellar bone with multiple, closely spaced growth marks resembling the EFS. The intensive remodeling observed in the smaller fibula is repeated in these larger specimens. Highly remodeled trabecular bone transitions smoothly into extensively remodeled cortices dominated by multiple generations of remodeling. Dense Haversian bone obliterates primary bone signatures throughout the cortex

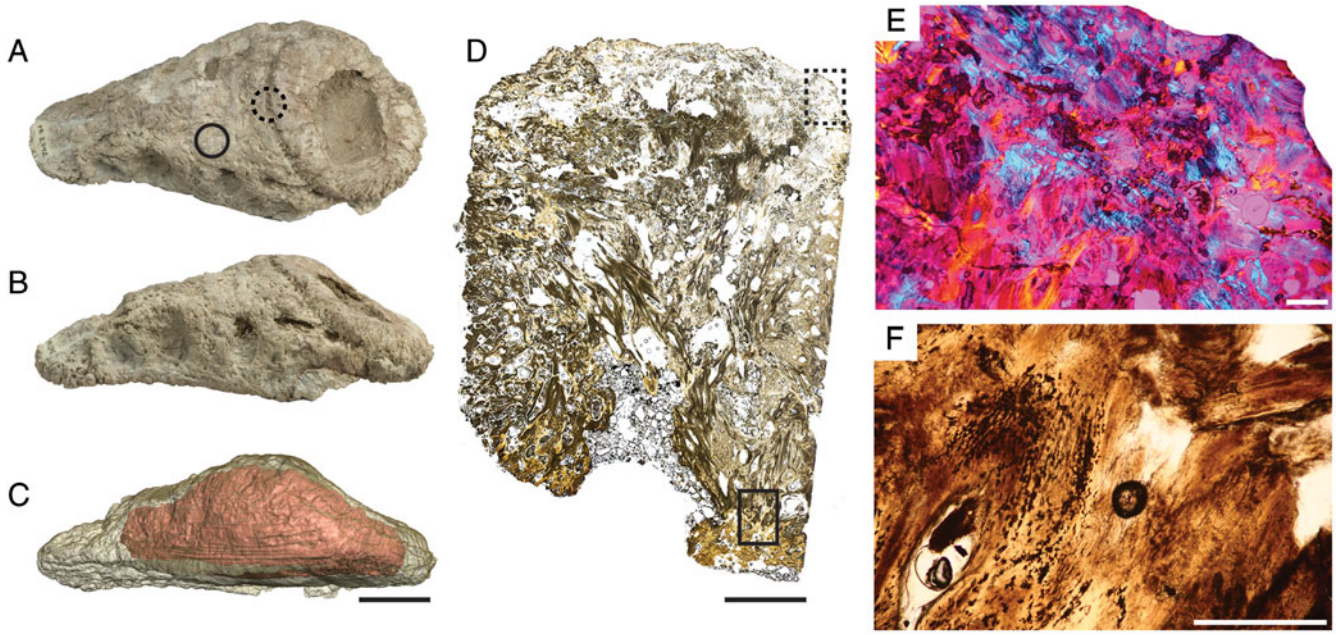

FIGURE 12. Microstructural organization of FMNH PR 2342, *Rapetosaurus krausei* osteoderm found in direct association with FMNH PR 2255, a 100% adult size partial postcranial skeleton, including the largest femur and rib described in this work. **A**, superficial view. Black solid circle indicates position of core for histology figured in **D**–**F**. Black dashed circle indicates position of thin-section taken from intersection of bulb root (Curry Rogers et al., 2011:fig. 1b). **B**, lateral view, illustrating surface texture, topography, and cingulum between bulb (toward right) and root (toward left). **C**, lateral view highlighting internal void identified by computed tomography (see Curry Rogers et al., 2011). **D**, general view of osteoderm histology in plain light at position of core indicated by black solid circle in **A**. Superficial surface is toward the top; deep surface bordering void is toward the bottom; dashed box indicates position of **E**; solid box indicates position of **F**. **E**, primary osseous matrix composed of structural fiber bundles in polarized light. Irregularly oriented sheets of lamellar bone characterize the external surface of the osteoderm. **F**, deeper regions of osteodermal bone in plain light exhibit irregularly oriented structural fiber bundles and some secondary osteonal bone surrounding vascular spaces. Scale bars equal 10 cm (**A**–**C**), 5 mm (**D**), and 500 μm (**E**, **F**).

in these larger fibulae (Fig. 8E). Irregular osteons do not occur in sampled fibulae over 50% adult size, and most secondary osteons are normal, with average diameters ca. 150–360 μm.

Ribs—Our sample includes four ribs ranging from 45% to 100% of adult size (Table 1). All histological samples come from the rib shaft distal to the tuberculum. *Rapetosaurus* ribs are pneumatized, and our samples highlight the extension of this pneumaticity into the rib shaft (Fig. 9C, E; Morphobank Project 2724).

The smallest sampled rib is associated with a juvenile *Rapetosaurus* skeleton mounted at the Field Museum of Natural History (FMNH PR 2209; Curry Rogers and Forster, 2001; Curry Rogers, 2009; Fig. 9A–C). Throughout the cortex, primary fibrolamellar bone is richly vascularized with longitudinal vascular canals (Fig. 9A, B). Within the woven bone scaffold of the fibrolamellar complex, osteocyte lacunae are dense and tightly packed (Fig. 9B). The external margin of this rib preserves an active growth front, with immature primary osteons (Fig. 9A, B). Several mid-cortical growth marks are present, but none can be traced circumferentially (Fig. 9A, B). They consist of thin zones of parallel-fibered bone and annuli surrounded by regions of fibrolamellar bone with longitudinal vascularity. The rib includes an open medullary space with thin bony trabeculae that record multiple layers of endosteally derived lamellae that have undergone multiple generations of remodeling (Fig. 9C). Sporadic occurrences of delicate fibers associated with secondary trabeculae and endosteal lamellae are consistent with the presence of air sacs (Lambertz et al., 2018) in this specimen. Primary bone in the deep cortex is overprinted by a single generation of remodeling recorded by immature, partially infilled secondary osteons and open resorption cavities (Fig. 9C). There are no irregular osteons or exceptionally large resorption cavities present in this element.

A complete section of a rib between 50% and 60% adult size preserves longitudinal fibrolamellar bone throughout the cortex (DMNH EPV.127350; Morphobank Project 2724). Two periosteal circumferential cracks may follow growth marks. Trabeculae consist of multiple layers of endosteally derived lamellar bone, and centripetal deposits of lamellar bone also line the medullary space. 'Pneumosteal bone' sensu Lambertz and colleagues (2018) is not observed in this element. Secondary remodeling obliterates primary bone in the deep cortex. Normal secondary osteons extend into the mid-cortex and occasionally reach the periosteal border. Irregular osteons are absent in this rib.

A partial section of a rib between 60% and 70% adult size retains primary bone in only a few small zones of longitudinal fibrolamellar tissue (UA 10012; Morphobank Project 2724). The external cortex captures primary longitudinal vascular canals, and immature primary osteons impart a scalloped morphology to the periosteal margin. Obliquely oriented vascular canals may indicate directional growth at the dorsal, periosteal border of the rib. Several growth marks in the mid- and external cortex are separated from one another by a few laminae of primary, fibrolamellar bone. These growth marks consist of up to seven stacked annuli and separate primary periosteal bone tissue from the remodeled deep and middle regions of the cortex. At least one morphologically similar growth mark is visible in patches beneath secondary osteons in the deeper cortex. Endosteal trabeculae are extensively remodeled and

transition to an extensively remodeled cortex with multiple generations of overlapping secondary osteons and resorption cavities extending into the outer cortex.

The largest rib is associated with the largest sampled femur (FMNH PR 2255) and a large osteoderm (FMNH PR 2342) and represents 100% adult size for the purposes of our study (Fig. 9D–F). The section is more distal than the others but retains medullary pneumaticity. Primary bone tissue is visible throughout the mid- and external cortex, where it is typically characterized by longitudinal primary osteons embedded in a woven bone scaffold (Fig. 9D, E). The external cortex preserves some regions of primary bone that are more highly vascularized with interweaving circular and longitudinal canals (Fig. 9D, E). Several growth marks are present near the periosteal surface, including some that are indicated by cracks in parallel with intact growth marks (Fig. 9D, E). These LAG are followed by deposition of longitudinal primary bone that varies from fibrolamellar to lamellar bone mineral organization depending on position (Fig. 9E). Peripheral growth marks cannot be termed an EFS in the context of ongoing periosteal bone apposition. Endosteal lamellar bone lines the large pneumatic fossae, and trabeculae have been intensely remodeled (Fig. 9F). Multiple overlapping generations of secondary osteons constitute dense Haversian bone in the perimedullar regions of the cortex. Some fine fibers integrated within this perimedullar secondary endosteal bone and deep secondary osteons may be osteological correlates of pneumaticity (Lambertz et al., 2018). More externally, secondary osteons occasionally remodel a single circumferential layer, as observed in some smaller appendicular elements (e.g., Figs. 2B, E, 5C–E, 6B, 9E). Irregular osteons are not present in this specimen.

Scapula—One scapula that is 32% adult size was analyzed in this study, with the thin-section positioned in the medial region of the scapula at the base of the scapular blade (Fig. 10; DMNH EPV.127476). The cortex is organized into at least nine distinctive cycles/modulations that are visible in gross view (Fig. 10A–C). These cycles are similar to the 'cycles' (Castanet et al., 1993; Rimblot-Baly et al., 1995; Curry, 1999) and the 'modulations' (Woodward and Lehman, 2009) described for other sauropod taxa. Where the scapular blade tapers, the bone depositional pattern shifts, probably as a reflection of a preferential anterior growth of the scapular spine. In this region, the anterior part of the scapular blade exhibits abundant primary vasculature, with primary osteons radiating away from the central trabecular space (Fig. 10A, B). Secondary osteons extend unevenly into the cortex, with clusters of immature secondary osteons overprinting primary tissue throughout the element, but most pervasive in the deep cortex. Bone remodeling in the mid-cortex is sometimes focused upon single circumferential layer and includes large, obliquely oriented resorption cavities (Fig. 10D).

Pubis—Thin-sections of the proximal pubic shaft from an individual of 68% adult size are poorly preserved but reveal a cross-section dominated by remodeling (Fig. 11A, B; DMNH EPV.127348). Along the periosteal edge, a circumferential layer of lamellar tissue with very sparse longitudinal primary osteons is preserved in a few areas. In some regions, the lamellar tissue is avascular (Fig. 11A). Dense Haversian bone extends from the deepest cortex to the periosteal surface and consists of overlapping generations of secondary osteons that are 100–200 μm in diameter and incorporate single Haversian canals. Irregular osteons are absent in this pubis (Fig. 11B).

Ischium—The proximal shaft of a 79% adult size ischium exhibits an osteohistology that is similar to that recorded in the pubis (Fig. 11C, D; DMNH EPV.127347). Multiple cycles of bone remodeling obscure any primary bone signal in all but the outermost cortex where a thin margin of avascularized primary lamellar bone persists on the lateral side of the element (Fig. 11C). Remodeling extends to the periosteal surface on the medial side of the ischium (Fig. 11D). Secondary osteons are normal throughout this specimen.

Osteoderm—The largest known *Rapetosaurus* individual (FMNH PR 2255) includes a separately catalogued osteoderm (Fig. 12; FMNH PR 2342) described in detail by Curry Rogers et al. (2011). Specimen FMNH PR 2342 was directly associated with the rib and femur sampled in this study, as well as with vertebrae, pelvic and pectoral elements, and limb bones that were not histologically sampled. The osteoderm exhibits a typical 'bulb and root' morphology (Le Loueff et al., 1994; D'Emic et al., 2009; Cerda et al., 2015b) and measures $57.2 \times 26.7 \times 19.2$ cm in maximum dimensions, with an estimated volume of 9.6 l, making it the among the most massive osteoderms known (Fig. 12A–C; Curry Rogers et al., 2011). Computed tomography indicates that FMNH PR 2342 exhibits an internal void approximately 4.9 l in volume, representing more than 50% of the total volume of the osteoderm (Fig. 12C; Curry Rogers et al., 2011).

Exploratory cores taken from the dorsal surface of the element indicate that the superficial surficial bone ranges from 1.2 to 3.5 cm in thickness (Fig. 12C, D; Curry Rogers et al., 2011). The core captures both the external region and deeper regions lining the internal void (Fig. 12D). The element is dominated by large, vascular spaces that are irregularly oriented. Where visible, primary bone tissue is composed of irregularly oriented, interwoven structural fiber bundles (= metaplastic bone; Cerda et al., 2015) that vary in diameter, length, and compactness (Fig. 12C, F). The external surface of the element preserves intersecting zones of irregularly oriented sheets of avascular lamellar bone (Fig. 12D, E). Secondary osteons are abundant throughout but vary in their orientations (Morphobank Project 2724). Fibrolamellar bone, growth marks, and 'pneumosteal tissue' (Lambertz et al., 2018) are absent (Fig. 12F).

DISCUSSION

Histological data provide direct evidence of the ontogenetic growth strategy of *Rapetosaurus krausei*. Our sample highlights microstructural variation among skeletal elements of similar relative size and within single elements throughout ontogeny. Some of these variations likely reflect the functional context of bone development. For example, all sampled girdle elements exhibit distinctive patterns of primary bone deposition and remodeling not shared by limb bones. Weight-bearing elements, including humeri (Fig. 2) and femora (Figs. 5, 6), exhibit well-vascularized fibrolamellar bone until very large sizes, whereas some non-weight-bearing elements (e.g., fibulae, pubis, ischium) exhibit nearly complete remodeling of the cortex by 60–70% adult size (e.g., Figs. 8, 10, 11). Mid-cortical modulations and endosteal remodeling help to distinguish ribs (Fig. 9) and scapulae (Fig. 10) from other appendicular elements. Although variations among skeletal elements exist, three main phases of osteogenesis characterize *Rapetosaurus* life history more broadly, and these are detailed below. New data presented here also shed light on a hypothesized novel 'titanosaurian growth strategy' (Stein et al., 2010; Company, 2011; Klein et al., 2012; García et al., 2015) and begin to help untangle the complex web of extrinsic factors, including paleoenvironment, that might influence bone growth in titanosaurs.

Growth in *Rapetosaurus*

Three osteogenic phases characterize *Rapetosaurus* life history. The first is recorded in elements approximately 40%

adult size or smaller (Table 1). In these bones, rapid sustained bone deposition is indicated by fibrolamellar primary bone dominated by longitudinal vascular canals and a general absence of growth marks. In some elements, and in some regions of many sampled elements, longitudinal vascular canals exhibit occasional radial and/or circular anastomoses. Woven bone scaffolds range, on average, between ca. 50 and 75 μm in thickness. Primary osteonal infills have radiuses ranging from ca. 150 to 225 μm on average and result in small primary osteon vascular canal diameters that impart a compaction of primary bone microstructure (Figs. 2A–C, 5A–C, 7A–C, 8). Compacted primary bone was also observed in neonatal *Rapetosaurus* (Curry Rogers et al., 2016) and is a common feature of *Rapetosaurus* bone microstructure at every size that we examined. In *Rapetosaurus* elements less than 40% adult size, the periosteal surfaces of bones record scalloped margins of open primary vascular spaces indicative of ongoing appositional growth (Figs. 2A, 5A, 7A, 8B, 9A, B). Intracortical and peripheral growth marks are generally absent in these small individuals, with the exception of LAG in a small tibia (UA 10013; Fig. 7A), rib (FMNH PR 2209; Fig. 9A), and primary bone cycles in a small scapula (Fig. 10A), which are similar to those observed in girdle elements of other sauropods (e.g., de Ricqlès, 1983; Rimblot-Baly et al., 1995; Curry, 1999; Sander, 2000; Lehman and Woodward, 2008). Bone remodeling begins soon after hatching in *Rapetosaurus* (Curry Rogers et al., 2016), and by early juvenile ontogenetic stages it extends as a single generation of resorption cavities and secondary osteons into the mid-cortex. Unusually large resorption cavities (~600–900 μm in diameter) are common to all *Rapetosaurus* limb elements of less than 40% adult size (Figs. 2B, 5C, 7B, 8C, 9A). These cavities often occur within a single mid-cortical layer, where they result in a circumferential band of intensive remodeling (e.g., Figs. 2B, 5C).

Individuals approximately 40–50% adult size document the second noteworthy osteogenic phase for *Rapetosaurus* because they record a temporary reduction in bone appositional growth rates. This reduction is heralded by a shift in bone structural organization in some limb elements. Primary fibrolamellar bone tissue still dominates the cortex (Figs. 5D–F, 7G, H), but in some elements (e.g., femur, fibula) longitudinally vascularized fibrolamellar bone grades into avascular lamellar bone with peripheral growth marks, reduced porosity, and more intense bone remodeling (Figs. 5D–F, 7G, H, 8A–C). Interestingly, if these peripheral growth marks were present in larger *Rapetosaurus* individuals, their stacked, sequential organization would potentially be diagnosed as the EFS. Their occurrence in these small *Rapetosaurus* individuals demands another explanation (see below).

Remodeling is pervasive in these juvenile elements, and evidence of this phenomenon extends well into the mid-cortex in circumferential bands, corresponding to the circumferential rows of resorption cavities noted in younger *Rapetosaurus* (Figs. 2B, 5C, 7B, E). The unusually large resorption cavities noted in the mid-cortices of younger *Rapetosaurus* appear to have undergone a single generation of remodeling, and the resultant secondary osteons are irregular (Figs. 5D–F, 7E, F, 8D, E). They capture multiple vascular bundles within a single external cementing line, exhibit an acellular lamella upon initial infilling, and reach average diameters more than 200–300 μm larger than normal secondary osteons. Irregular osteons regularly exceed long-axis diameters of 800 μm and are only present in *Rapetosaurus* individuals of approximately 40–50% adult size. For comparison, secondary osteon diameters in humans range from 150 to 350 μm (Agerbaek et al., 1991; Brockstedt et al., 1996; Currey, 2002; Van Oers et al., 2008).

Later-stage *Rapetosaurus* ontogenetic growth strategy is illustrated by individuals approximately 60% adult size and larger. Resumed appositional growth is evidenced by the deposition of longitudinal fibrolamellar bone. In some elements, slower-growing lamellar-zonal bone with sparse longitudinal primary osteons persists in the peripheral cortices (e.g., Figs. 3C, D, 4A, B, 6, 8E, 9D, E, 10, 11). Some sampled elements retain only small patches of longitudinally vascularized lamellar primary bone visible beneath dense Haversian remodeling (e.g., fibula, Fig. 8E; pubis, Fig. 11A). Mid-cortical growth marks are common in these larger individuals, with some elements depositing abundant peripheral/external cortical growth marks. The EFS is absent in the largest known *Rapetosaurus* (Figs. 6, 9D–F), indicating ongoing appositional growth. Remodeling is pervasive for *Rapetosaurus*, starting in individuals only 50% adult size, but the intensity of remodeling is element dependent: dense Haversian bone nearly replaces primary tissue in fibulae (Fig. 8), the pubis (Fig. 11A), and the ischium (Fig. 11B) in specimens between 60% and 80% adult size. Irregular osteons are absent from larger individuals, presumably because repeated cycles of remodeling have replaced them with more typical secondary osteons (e.g., Figs. 2E, F, 6, 8E).

Bulb and root osteoderms similar to FMNH PR 2342 are widespread among titanosaurs (Csiki, 1999; Salgado et al., 2005; D'Emic et al., 2009; Cerda and Powell, 2010; Carrano and D'Emic, 2015; Cerda et al., 2015b; Vidal et al., 2017). Although general microstructural organization is generally consistent among sampled osteoderms (e.g., Cerda and Powell, 2010; Cerda et al., 2015), only a handful of known osteoderms exhibit large internal voids like that described for *Rapetosaurus* (Curry Rogers et al., 2011; Vidal et al., 2017). Titanosaur osteoderms undoubtedly served multiple functions consistent with their diversity of form (e.g., D'Emic et al., 2009; Cerda et al., 2015b), not the least of which may have been as a reserve of labile mineral resources within the dermis (Curry Rogers et al., 2011; Cerda et al., 2015b; Vidal et al., 2017).

Rapetosaurus ontogenetic growth is similar to that previously documented in other large-bodied titanosaurs, including *Alamosaurus* (Woodward and Lehman, 2009; Klein et al., 2012) and *Bonitasaura* (Gallina, 2012). Patterns of *Rapetosaurus* growth also resemble the general patterns observed in non-titanosaur neosauropods and extant large-bodied mammals (e.g., Enlow and Brown, 1958; Frylestam and Schantz, 1977; Cormack, 1991; Klevezal, 1996; Curry, 1999; Sander, 2000; Sander et al., 2004, 2011; Klein and Sander, 2008; Lehman and Woodward, 2008; Sander and Clauss, 2008; Zedda et al., 2008; Woodward and Lehman, 2009; Curtin et al., 2012; Klein et al., 2012; Mitchell and Sander, 2014; Nganvongpanit et al., 2016). Like *Rapetosaurus*, these taxa exhibit a bone growth pattern characterized by continuous deposition of highly vascularized primary fibrolamellar bone that transitions to more organized, slower bone deposition. These taxa also undergo regular cycles of remodeling until late in ontogeny, when an EFS signals the attainment of maximum body size (e.g., Cormack, 1991; Klevezal, 1996; Curry, 1999; Sander, 2000; Woodward and Lehman, 2009). *Rapetosaurus* also shares compacted primary osteons and an early onset of secondary remodeling with all titanosaurs studied from a histological perspective (Cerda and Powell, 2009; Klein et al., 2009, 2012; Woodward and Lehman, 2009; Stein et al., 2010; Cerda and Salgado, 2011; Company, 2011; Gallina, 2012; Lacovara et al., 2014; García et al., 2015; Chinsamy et al., 2016; Carballido et al., 2017). That said, *Rapetosaurus* also exhibits interesting features that differ from those previously described. These are discussed in more detail below.

Noteworthy Aspects of *Rapetosaurus* Growth

Compacted Primary Fibrolamellar Bone—Compacted highly vascularized fibrolamellar primary bone tissue may be unique to titanosaurs (Woodward and Lehman, 2009), and in at least a few titanosaur taxa the scaffold of the fibrolamellar complex is modified and deposited as "parallel-fibered or lamellar bone instead of woven bone" (Klein et al., 2012:11). Klein and colleagues (2012) formalized this potentially novel tissue type as 'modified laminar bone' (MLB) and postulated that MLB might reflect a reduced primary bone growth rate in *Phuwiangosaurus* (Klein et al., 2009), *Magyarosaurus* (Stein et al., 2010), *Lirainosaurus* (Company, 2011), and *Ampelosaurus* (Klein et al., 2012). In their characterization of MLB, Klein et al. (2012:11) noted the complex nature of this bone tissue and warned that "high amounts of parallel-fibered and lamellar bone matrix in the scaffolding should not be confused with particularly well developed primary osteons that form only after the deposition of the scaffolding." These authors also recognized the inconsistency between their hypothesis of slowed deposition for MLB and the dense vascular networks that characterize all sampled titanosaurs (Klein et al., 2012). Klein et al. (2012:16) concluded that "a more comprehensive sampling of titanosaurs" would help resolve outstanding questions related to MLB, including whether the proposed shift in bone microstructural organization reflects a slowed rate of primary bone deposition.

Our data for *Rapetosaurus* indicate that highly vascularized fibrolamellar bone tissue with a woven bone scaffold is present throughout ontogeny. The woven bone scaffold represents the first pulse of growth and sets the baseline for appositional rate (Francillon-Viellot et al., 1990). In *Rapetosaurus* (and *Alamosaurus*; Woodward and Lehman, 2009; Klein et al., 2012), wide vascular spaces are captured by the appositional front and these spaces are infilled with thick deposits of lamellar bone (e.g., Curry, 1999; Sander, 2000; Sander et al., 2011). This process effectively compacts the primary bone tissue because vascular spaces are narrowed. Once infilled, the overwhelming formation of compacted primary osteons formed by circumferential deposits of lamellar bone in *Rapetosaurus* could make it easy to overlook the intervening woven bone scaffold (e.g., Fig. 5A, B). In the *Rapetosaurus* sample, woven bone constitutes the scaffolding of the fibrolamellar complex even in the largest specimens (Figs. 6, 9D–F). We contend that the hypothesized occurrence of MLB in other taxa is likely an error related to diagenesis or mistaking the lamellar bone infilling primary osteons for periosteal appositional bone.

Lastly, experimental data demonstrate that the continuum of bone tissue vascular patterns (e.g., laminar, reticular, longitudinal vascularity) can be associated with a wide range of bone growth rates depending upon the element under scrutiny, biomechanics, individual age, resting metabolic rate, environmental conditions, and phylogenetic history (e.g., Amprino, 1947; Castanet et al., 2000; de Margerie, 2002; de Margerie et al., 2002, 2004; Starck and Chinsamy, 2002; Sander and Tückmantel, 2003; Castanet et al., 2004; Chinsamy-Turan, 2005; de Boef and Larsson, 2007; Cubo et al., 2008, 2012; Montes et al., 2010). In order to develop hypotheses for estimating bone growth rates from bone histological traits, Cubo et al. (2012) employed a sample of extant amniotes and developed a model that they applied to a range of extinct archosaurs. Their data suggest that elevated growth rates are basal for Dinosauria and are highest among saurischian dinosaurs, including sauropodomorphs (Cubo et al., 2012). Densely vascularized fibrolamellar primary bone in *Rapetosaurus* is consistent with relatively fast appositional bone growth throughout ontogeny, in all sampled elements in which primary bone persists, just as it is among many extant, rapidly growing amniotes (e.g., Stover et al., 1992; Klevezal, 1996; Castanet et al., 2000; de Margerie, 2002; de Margerie et al., 2002, 2004; Starck and Chinsamy, 2002; Cubo et al., 2008, 2012; Zedda et al., 2008; Montes et al., 2010; Curtin et al., 2012; Nganvongpanit et al., 2016).

Early Ontogeny Peripheral Growth Marks—Periosteal growth marks indicate intervals of decreased growth rate (annuli) or dormancy (LAG) in extant vertebrates and are employed in skeletochronological studies of extant animals and dinosaurs (e.g., Enlow and Brown, 1956, 1957, 1958; Morris, 1970; Hutton, 1986; Castanet et al., 1993, Castanet, 1994, 2004; Klevezal, 1996; Horner et al., 1999; Currey, 2002; de Ricqlès et al., 2004; Erickson et al., 2004; Bybee et al., 2006; Ostrowski et al., 2006; Köhler et al., 2012; Lee and O'Connor, 2013; Woodward et al., 2013, 2015). In living ectotherms, these growth marks often occur in the context of slowly formed lamellar bone. In extant endotherms, cyclical growth marks within fast-growing fibrolamellar bone are typically inferred to relate to the energetic challenges of the dry season (e.g., Turvey et al., 2005; Ostrowski et al., 2006; Sander and Andrassy, 2006; Köhler and Moyà-Solà, 2009; Köhler et al., 2012; Straehl et al., 2013). In fact, growth patterns in ruminants are finely tuned to seasonal resources availability, with high rates of fibrolamellar bone apposition linked to intervals of rapid growth when food resources are abundant (Jha et al., 1968; Arendt and Reznick, 2005; Sander and Klein, 2005; Köhler et al., 2012; Curtin et al., 2009; 2012; Marín-Moratalla et al., 2014). LAG signal intervals of resource instability, coinciding with lowered food intake and higher rates of mortality (e.g., Köhler et al., 2012). Later in ontogeny, tightly spaced growth lines in a context of slow-growing avascular lamellar bone at the external margins of appendicular elements are called the EFS and signal a growth plateau in adults with a determinate growth strategy (Klevezal et al., 1972; Chinsamy, 1990; Cormack, 1991; de Ricqlès et al., 2004; Ponton et al., 2004; Sander et al., 2006; Woodward et al., 2011; Lee and O'Connor, 2013).

Among sauropods, cyclical mid-cortical growth marks are usually absent, but when they occur they are either similar to LAG deposited in ruminants or they are deposited as cyclical 'modulations' or 'polish lines' that lack bounding LAG (de Ricqlès, 1983; Rimblot-Baly et al., 1995; Curry, 1999; Sander, 2000; Klein and Sander, 2008; Woodward and Lehman, 2009; Sander et al., 2011). In most sauropod limb elements, the first cortical growth marks occur late in ontogeny and are typically interpreted as the EFS (Curry, 1999; Sander, 2000; Klein and Sander, 2008). Among titanosaurs, cortical growth marks are most common in larger individuals (e.g., Klein et al., 2009; Company, 2011) where they are thought to signal slowed appositional growth associated with skeletal maturity (e.g., Castanet et al., 1993; Curry, 1999; Sander, 2000; Klein and Sander, 2008; García et al., 2015; Carballido et al., 2017; Cerda et al., 2017). These growth marks have been interpreted as the EFS in just a few titanosaurs (Cerda and Powell, 2009; Woodward and Lehman, 2009; Cerda and Salgado, 2011; Cerda et al., 2015; García et al., 2015), indicating that most titanosaurs studied so far were still growing. Our data indicate that the largest known *Rapetosaurus* (Figs. 5G–I, 8D–F) had not yet reached asymptotic sizes (e.g., Castanet et al., 1993; de Ricqlès et al., 2004; Klein et al., 2012; García et al., 2015).

Rapetosaurus exhibits an interesting mid-ontogeny pause in primary bone depositional rates that differs from the condition in most other described sauropods. Peripheral growth marks comparable to the EFS are deposited in small individuals (~50% adult size or smaller; Figs. 5D–F, 6, 7A). If observed later in ontogeny, these structures would be diagnosed as the EFS, particularly when considered in combination with

pervasive bone remodeling (see below). If our sample had only included relatively small *Rapetosaurus* specimens, it would have been reasonable to conclude that *Rapetosaurus* had experienced a shift in ontogenetic growth strategy that truncated primary growth and led to the evolution of dwarfism akin to the pattern documented in *Magyarosaurus* (Stein et al., 2010). However, our ontogenetic sample reveals that the slowing of bone apposition in juvenile *Rapetosaurus* was temporary, because more active bone deposition is recorded in later ontogenetic stages.

We hypothesize that the widespread presence of peripheral LAG in young *Rapetosaurus* may correspond to the temporary cessation of growth related to resource limitations in the Maevarano Formation paleoenvironment, and are consistent with the annuli deposited in extant large-bodied mammals that live through an interval of environmental stress (Jha et al., 1968; Lawler and White, 1997; McNab, 2002; Ostrowski et al., 2006; Curtin et al., 2009; Köhler et al., 2012; Straehl et al., 2013; Marín-Moratalla et al., 2014). This reconstruction is consistent with sedimentological and taphonomic data that suggest that the Maevarano Formation accumulated under a seasonal, semiarid climatic regime that prompted recurrent drought-related mortality (Rogers et al., 2000, 2007; Rogers, 2005; Krause et al., 2010). Juvenile *Rapetosaurus* are among the most common components of the many Maevarano death assemblages, and this fact may signal their susceptibility to resource-related stress during recurrent droughts. The record clearly indicates that many juvenile *Rapetosaurus* individuals fell victim to drought (or perhaps another killing agent). Those that survived (and those that didn't experience lethal events) presumably resumed higher growth rates on the path to adulthood. This reconstruction is supported by the presence of highly vascularized fibrolamellar bone deposition in older *Rapetosaurus* individuals. In these older individuals, bone tissue indicates that growth rates continued unabated with increasing size/age and that the largest known *Rapetosaurus* individual was still actively growing at the time of death. As for most other titanosaurs (e.g., García et al., 2015; Carballido et al., 2017), the absence of the EFS in the largest sampled elements indicates that we do not yet know the asymptotic body size for *Rapetosaurus*.

Early Intensive Bone Remodeling—Bone remodeling occurs throughout life and at variable rates throughout the vertebrate skeleton and is related to several interrelated metabolic and mechanical functions: (1) removing injured bone tissue that has accumulated microscopic fractures (Mori and Burr, 1993; Burr, 2002; Currey, 2002; Martin 2003; Brianza et al., 2011); (2) reinforcing and remobilizing bone tissue in areas of loading/stress (Lanyon and Baggot, 1976; Carrier and Leon, 1990; Pfeiffer et al., 2006; McFarlin et al., 2008; Skedros et al., 2013); (3) regulating calcium homeostasis (Mundy, 1987; Parfitt, 1987; Dempster, 1992; McCarthy and Frasscia, 1998; Currey et al., 2016); and (4) maintaining osteocyte viability (Currey et al., 2016). Bone remodeling results in the formation of secondary osteons. The spatial dimensions of secondary osteons have been analyzed for humans and various other mammalian species (Agerbaek et al., 1991; Brockstedt et al., 1996; Havill, 2003; Mori et al., 2005; Pfeiffer et al., 2006; McFarlin et al., 2008; Van Oers et al., 2008; Zedda et al., 2008; Skedros et al., 2013; Currey et al., 2016; Nganvongpanit et al., 2016; Felder et al., 2017). Among mammals, mean resorption area and Haversian canal area scale with negative allometry (Felder et al., 2017): biomechanical constraints drive osteon dimensions in small animals, whereas osteocyte viability dictates osteon dimensions in large animals (Felder et al., 2017). Osteocyte viability in extant mammals is compromised when distanced more than ca. 230 μm from a blood supply, resulting in secondary osteon diameters typically being limited to ca. 150–350 μm, and rarely approaching a maximum of ca. 580 μm in extant mammals (Lozupone and Favia, 1990; Felder et al., 2017).

Evidence of bone remodeling is common among sauropods, where later ontogenetic stages are generally characterized by pervasive cycles of bone resorption and redeposition that yield multiple, overlapping generations of secondary osteons (dense Haversian bone) (e.g., Sander et al., 2011). Among non-titanosaurian sauropods, patterns of bone remodeling have been used as relative age indicators ('histologic ontogenetic stages,' HOS; Klein and Sander, 2008), and this approach is particularly useful in animals that lack regular annual growth marks.

Extensive remodeling of primary bone begins in early ontogeny for all described titanosaurs, including *Rapetosaurus* (Klein and Sander, 2008; Klein et al., 2009, 2012; Woodward and Lehman, 2009; Stein et al., 2010; Company, 2011; Sander et al., 2011; Gallina, 2012; Cerda et al., 2014, 2017; García et al., 2015; Chinsamy et al., 2016; Curry Rogers et al., 2016). High rates of remodeling are thought to overtake primary bone depositional rates in early ontogeny in *Phuwiangosaurus* and *Magyarosaurus*, which are hypothesized to have reduced primary growth rates (Klein et al., 2009, 2012; Stein et al., 2010). In other titanosaurs, such as *Ampelosaurus*, secondary remodeling begins later in ontogeny but soon overtakes periosteal growth, potentially highlighting rapid rates of bone remodeling (Klein et al., 2012). *Rapetosaurus*, *Alamosaurus, Epachthosaurus* and *Lirainosaurus* exhibit extensive early ontogeny remodeling and record concentrated 'bands' of bone remodeling that may follow single layers (*Rapetosaurus*, *Lirainosaurus*, *Epachthosaurus*) or 'modulations' within primary bone (*Alamosaurus*) (Woodward and Lehman, 2009). This pattern has also been observed in earlier sauropod dinosaurs (e.g., *Leyesaurus*; Cerda et al., 2017), where they commonly coincide with growth marks. Intense secondary remodeling throughout *Rapetosaurus* ontogeny, including in neonates (Curry Rogers et al., 2016), supports the notion that the process is not merely size-dependent (Garcia et al., 2015).

The early onset of intense remodeling may be unique to titanosaurs and prohibits a simple application of unmodified HOS categories (Stein et al., 2010; Company, 2011; Klein et al., 2012). The mid-ontogeny pause in primary bone apposition and pervasive remodeling of the external cortex in early *Rapetosaurus* ontogeny results in a mismatch between HOS stage and the small size of sampled specimens. Even if we used the modified HOS approach suggested by other titanosaur workers (Stein et al., 2010; Klein et al., 2012), our sample would yield 'adult' *Rapetosaurus* HOS and bone tissue type indicators at less than 50% adult size (e.g., Figs. 5D–F, 6D–F). Moreover, at the other end of the ontogenetic spectrum (adult individuals), primary bone deposition, more limited external cortical remodeling, and the lack of a definitive EFS would result in younger HOS and bone tissue types for the biggest elements sampled (e.g., Fig. 6). In light of these complications, we have not used the existing HOS approach to categorize bone tissue types in the *Rapetosaurus* sample.

In any case, *Rapetosaurus* offers a broadened perspective on the early signals of bone remodeling, which are present even in neonates (Curry Rogers et al., 2016). The early initiation of remodeling in *Rapetosaurus* sometimes results in unusually large resorption cavities (~600–800 μm in diameter) in the midcortices of sampled small juvenile limb elements (Figs. 2B, C, 5B, C, 7B, C). These erosional cavities are replaced by irregular osteons characterized by diameters exceeding 600 μm (many in excess of 800 μm) with multiple vascular bundles (Figs. 5E, F, 7D–F, 8B, C). Irregular osteons occur alongside typical secondary osteons in small individuals but are presumably obliterated by successive generations of secondary

remodeling in later ontogeny (e.g., Figs. 5G–I, 6, 7G–I, 8E). It is important to note that unusually large resorption cavities and irregular osteons occur in different *Rapetosaurus* limb elements from disparate localities, each representing a single individual. This pattern of occurrence negates the premise that these features relate to specific functional microenvironments or are unique to a single pathological individual.

The underlying reason(s) for the presence of unusual osteons in the *Rapetosaurus* sample remains unknown, although studies of extant animals may provide some insights. For example, large osteons may be advantageous for resisting bending and compression loads (Currey, 2002; Martin, 2003; Van Oers et al., 2008; Martin et al., 2015; Currey et al., 2016), perhaps indicating that the unusual pattern of bone remodeling in *Rapetosaurus* relates to an unknown biomechanical demand specific to small juveniles. That said, large irregular osteons are presently undocumented in larger individuals, where such loads would likely have increased with body mass (Brianza et al., 2011; Dempster, 1992; Havill, 2003; Van Oers et al., 2008; Skedros et al., 2013; Felder et al., 2017).

Unusually large cortical resorption cavities and corresponding "unusually large" secondary osteons (Young et al., 1986:109) have also been described in the veterinary literature (e.g., Landry and Fleisch, 1964; Jowsey and Johnson, 1972; Schock et al., 1975; Young et al., 1979, 1983, 1986; Young and Schneider, 1981; Wronski and Morey, 1983; Weinreb et al., 1989; Smith, 1994). These studies of chronic immobilization in mammals found that rapid bone loss caused by unregulated osteoclastic resorption of cortical bone tissue resulted in resorption cavities with diameters of 500–1500 μm (summarized in McCarthy and Frassica, 1998). If organisms survived the temporary increase in bone porosity dictated by this excessive remodeling, secondary osteons with mean wall thicknesses "2–3 times larger than normal" (Young et al., 1986:109) formed after several months of recovery. Because osteocyte viability is compromised with increasing distance from vascular supplies (Lozupone and Favia, 1990; Felder et al., 2017), later cycles of remodeling would likely result in reduced osteon dimensions and a more stable microstructural organization (Van Oers et al., 2008; Martin et al., 2015; Currey et al., 2016; Felder et al., 2017). Similar patterns of intensive intracortical remodeling have also been noted in vitamin D deficient extant vertebrates, with irregular patterns of bone mineral mobilization when blood calcium and phosphorous levels are disrupted as a result of physiological stress, including starvation and illness (Belanger, 1969; Jowsey and Johnson, 1972; Martin and Armelagos, 1985; Parfitt, 1987; Smith, 1994; McCarthy and Frassica, 1998; Curtin et al., 2012).

Although the exact cause(s) of the unusual osteons in juvenile *Rapetosaurus* individuals remains unknown, it is logical to evaluate them in a common-cause context. The documented pattern of widespread intensive remodeling and irregular osteons may illustrate another microstructural response to the seasonal nutritional stress that plagued the Maevarano Formation ecosystem. With resource limitations during drought (e.g., Rogers et al., 2003, 2007; Rogers, 2005), rapidly growing juvenile *Rapetosaurus* individuals likely experienced deficiencies in critical bone-building nutrients (e.g., Pratt and McCance, 1960; Belanger, 1969; Jowsey and Johnson, 1972; Mundy, 1987; Parfitt, 1987; Smith, 1994; McCarthy and Frassica, 1998). Perhaps concentrated osteoclastic activity focused on the mobilization of calcium and phosphorus reserves in bone yielded the large voids we observed in early juvenile *Rapetosaurus*. If impacted individuals survived, later deposition of irregular osteons would stabilize bone microstructure during a posterosional recovery phase (e.g., Bernhard et al., 2013; Currey and Shahar, 2013). Osteocyte viability at the margins of these large osteons would require additional vasculature, prompting the inclusion of multiple capillaries within single secondary osteons. Later in *Rapetosaurus* ontogeny, more regular patterns of bone appositional growth remodeling could resume, resulting in general replacement of the unusual signals of earlier ontogeny with dense Haversian bone composed of normal secondary osteons.

CONCLUSIONS

Our analysis of the bone histology in 23 individuals of *Rapetosaurus krausei* spans nine appendicular elements across a full ontogenetic range (from neonates to adults). *Rapetosaurus* shares highly vascularized primary fibrolamellar bone with other large-bodied sauropod dinosaurs, including the titanosaurs *Alamosaurus*, *Lirainosaurus*, and *Phuwiangosaurus*. Like these titanosaurs, *Rapetosaurus* exhibits compacted primary osteons, but woven bone scaffolding persists within the fibrolamellar framework and is consistent with overall high rates of bone apposition throughout most of ontogeny. *Rapetosaurus* growth rates transition over the course of ontogeny, and in large individuals signals of appositional decrease become more apparent. Interestingly, the largest known *Rapetosaurus* in our sample (femur length = 143 cm) was still growing, whereas some much smaller individuals illustrate a pause in primary osteogenesis. Secondary remodeling is pervasive in *Rapetosaurus* and other titanosaurs beginning in early ontogeny and can obliterate primary bone signals even in individuals that are less that 60% adult size.

Several aspects of *Rapetosaurus* bone tissue are distinctive. First, in elements less than 40% adult size, osteoclastic resorption has eroded vacuous cavities within mid-cortical primary fibrolamellar bone. At ontogenetic stages between 40% and 50% adult size, these cavities are often infilled with irregular osteons (with multiple included capillaries) exhibiting diameters two to three times larger than normal secondary osteons. At similarly small juvenile ontogenetic stages, peripheral growth marks comparable to the EFS accompany a shift to slower-growing, poorly vascularized lamellar primary bone that together indicate a temporary cessation in bone growth. In animals larger than 50% adult size, more rapid primary growth resumes, and early ontogeny peripheral growth marks and irregular osteons are replaced by overlapping generations of normal secondary osteons. We propose that these unusual signals may be explained as a response to the chronic resource challenges posed by the Maevarano Formation paleoenvironment.

ACKNOWLEDGMENTS

Members of the Mahajanga Basin Project collected the specimens described in this report between 1993 and 2010. L. Ballewske, D. Sorenson, and M. Whitney, all Macalester College alumni, contributed to preliminary data collection. J. Thole and K. Moffat provided microscopy and photography assistance. W. Simpson provided ready access to materials held in the Field Museum of Natural History collections. R. Rogers and M. D'Emic provided comments on earlier drafts of this paper. Thoughtful reviews by I. Cerda and E. Prondvai greatly improved the quality of the manuscript. Grants from the National Science Foundation (EAR-0955716, DEB-0822957, EAR-1664432, EAR-9418816, EAR-9706302, and EAR-0446488) and the National Geographic Society (8597-09) supported this work.

LITERATURE CITED

Agerbaek, M. O., E. F. Ericksen, J. Kragstrup, L. Mosekilde, and F. A. Melsen. 1991. A reconstruction of the bone remodeling cycle in a normal human cortical iliac bone. Bone and Mineral 12:101–112.

Amprino, R. 1947. La structure du tissue osseux envisagé comme expression de différences dans la vitesse de l'accroissement. Archives de Biologie 58:315–330.

Arendt, J. D., and D. N. Reznick. 2005. Evolution of juvenile growth rates in female guppies (*Poecilia reticulata*): predator regime or resource level? Proceedings of the Royal Society of London B, Biological Sciences 272:333–337.

Belanger, L. F. 1969. Osteocytic osteolysis. Calcified Tissue Research 4:1–12.

Benson, R. B. J., G. Hunt, M. Carrano, and N. Campione. 2018. Cope's rule and the adaptive landscape of dinosaur body size evolution. Palaeontology 61:13–48.

Benson, R. B. J., N. E. Campione, M. T. Carrano, P. D. Mannion, C. Sullivan, P. Upchurch, and D. C. Evans. 2014. Rates of dinosaur body mass evolution indicate 170 million years of sustained ecological innovation on the avian stem lineage. PLoS Biology 12:e1001853.

Bernhard, A., P. Milovanovic, E. A. Zimmermann, M. Hanh, D. Djonic, M. Krause, S. Breer, K. Püschel, M. Djuric, M. Amling, and B. Busse. 2013. Micro-morphological properties of osteons reveal changes in cortical bone stability during aging, osteoporosis, and bisphosphonate treatment in women. Osteoporosis International 24:2671–2680.

Bonaparte, J. F., and J. E. Powell. 1980. A continental assemblage of tetrapods from the Upper Cretaceous of Northwestern Argentina (Sauropoda-Ceolurosauria-Carnosauria-Aves). Mémories de la Société Géologique de France 139:19–28.

Brianza, S. Z. M., P. D'Amelio, N. Pugno, E. Zini, A. Zatelli, F. Pluviano, K. Cabiale, M. Galloni, and G. C. Isaia. 2011. Microdamage accumulation changes according to animal mass: an intraspecies investigation. Calcified Tissue International 88:409–415.

Brockstedt, H., J. Bollerslev, F. Melsen, and L. Mosekilde. 1996. Cortical bone remodeling in autosomal dominant osteopetrosis: a study of two different phenotypes. Bone 18:67–72.

Burr, D. B. 2002. Targeted and non-targeted remodeling. Bone 30:2–4.

Bybee, P. J., A. H. Lee, and E. Lamm. 2006. Sizing the Jurassic theropod dinosaur *Allosaurus*: assessing growth strategy and evolution of ontogenetic scaling of limbs. Journal of Morphology 267:347–359.

Carballido, J. L., D. Pol, A. Otero, I. A. Cerda, L. Salgado, A. C. Garrido, J. Ramezani, N. R. Cúneo, and J. M. Krause. 2017. A new giant titanosaur sheds light on body mass evolution among sauropod dinosaurs. Proceedings of the Royal Society B, Biological Sciences 284:20171219. doi: 10.1098/rspb.2017.1219.

Carrano, M. T., and M. D. D'Emic. 2015. Osteoderms of the titanosaur sauropod dinosaur *Alamosaurus sanjuanensis* Gilmore, 1922. Journal of Vertebrate Paleontology. doi: 10.1080/02724634.2014.901334.

Carrano, M. T., S. D. Sampson, and C. A. Forster. 2002. The osteology of *Masiakasaurus knopfleri*, a small abelisauroid (Dinosauria: Theropoda) from the Late Cretaceous of Madagascar. Journal of Vertebrate Paleontology 22:510–534.

Carrier, D., and L. R. Leon. 1990. Skeletal growth and function in the California gull (*Larus californicus*). Journal of Zoology 222:375–389.

Castanet, J. 1994. Age estimation and longevity in reptiles. Gerontology 40:174–192.

Castanet, J., K. Curry Rogers, and J. Cubo. 2000. Periosteal bone growth rates in extant ratites (ostrich and emu). Implications for assessing growth in dinosaurs. Comptes Rendus de l'Académie des Sciences, Series III, Sciences de la Vie 323:543–550.

Castanet, J., H. Francillon-Vieillot, F. J. Meunier, and A. J. de Ricqlès. 1993. Bone and individual aging; pp. 245–283 in B. K. Hall (ed.), Bone, Volume 7: Bone Growth—B. CRC Press, Boca Raton, Florida.

Castanet, J., S. Croci, F. Aujard, M. Perret, J. Cubo, and E. de Margerie. 2004. Lines of arrested growth in bone and age estimation in a small primate: *Microcebus murinus*. Journal of Zoology 263:31–39.

Cerda, I. A., and J. E. Powell. 2009. Patrón de crecimiento de *Saltasaurus loricatus* Bonaparte y Powell 1981 (Sauropoda: Titanosauria) inferido a partir de su histología ósea. Ameghiniana, Suplemento Resúmenes 46:68R.

Cerda, I. A., and J. E. Powell. 2010. Dermal armor histology of *Saltasaurus loricatus,* an Upper Cretaceous sauropod dinosaur from Northwest Argentina. Acta Paleontologica Polonica 55:389–398.

Cerda, I. A., and L. Salgado. 2011. Bone microstructure of the Upper Cretaceous titanosaur sauropod *Neuquensaurus australis* Lydekker, 1893. Ameghiniana, Suplemento Resúmenes 48:98R–99R.

Cerda, I. A., A. Chinsamy, and D. Pol. 2014. Unusual endosteally formed bone tissue in a Patagonian basal sauropodomorph dinosaur. The Anatomical Record 297:1385–1391.

Cerda, I. A., G. Casal, R. Martínez, and L. Ibiricu. 2015a. Histological evidence for a supraspinous ligament in sauropod dinosaurs. Royal Society Open Science 2:150369, doi: 10.1098/rsos.150369.

Cerda, I. A., R. A. García, J. E. Powell, and O. Lopez. 2015b. Morphology, microanatomy, and histology of titanosaur (Dinosauria, Sauropoda) osteoderms from the Upper Cretaceous of Patagonia. Journal of Vertebrate Paleontology. doi: 10.1080/02724634.2014.905791.

Cerda, I. A., A. Chinsamy, D. Pol, C. Apaldetti, A. Otero, J. E. Powell, and R. N. Martínez. 2017. Novel insight into the origin of the growth dynamics of sauropod dinosaurs. PLoS ONE 12:e0179707. doi: 10.1371/journal.pone.0179707.

Chinsamy, A. 1990. Physiological implications of the bone histology of *Syntarsus rhodesiensis* (Saurischia: Theropoda). Palaeontologia africana 27:77–82.

Chinsamy, A., I. Cerda, and J. Powell. 2016. Vascularized endosteal bone in armoured sauropod dinosaurs. Scientific Reports 6:24858, doi: 10.1038/srep24858.

Chinsamy-Turan, A. 2005. The Microstructure of Dinosaur Bone: Deciphering Biology with Fine-scale Techniques. The Johns Hopkins University Press, Baltimore, Maryland, 195 pp.

Company, J. 2011. Bone histology of the titanosaur *Lirainosaurus astibiae* (Dinosauria: Sauropoda) from the latest Cretaceous of Spain. Naturwissenschaften 98:67–78.

Cormack, D. H. 1991. Essential Histology. Lippincott, Williams, and Wilkins, Philadelphia, Pennsylvania, 345 pp.

Csiki, Z. 1999. New evidence of armoured titanosaurids in the Late Cretaceous—*Magyarosaurus dacus* from the Hateg Basin (Romania). Oryctos 2:93–99.

Cubo, J., N. Le Roy, C. Martinez-Maza, and L. Montes. 2012. Paleohistological estimation of bone growth rate in extinct archosaurs. Paleobiology 38:335–349.

Cubo, J., P. Legendre, A. J. de Ricqlès, L. Montes, E. de Margerie, J. Castanet, and Y. Desdevises. 2008. Phylogenetic, functional, and structural components of variation in bone growth rates of amniotes. Evolution and Development 10:217–277.

Currey, J. D. 2002. Bones: Structure and Mechanics. Princeton University Press, Princeton, New Jersey, 436 pp.

Currey, J. D., and R. Shahar. 2013. Cavities in the compact bone in tetrapods and fish and their effect on mechanical properties. Journal of Structural Biology 183:107–122.

Currey, J. D., M. N. Dean, and R. Shahar. 2016. Revisiting the links between bone remodeling and osteocytes: insights from across phyla: what is bone remodeling for? Biological Reviews. doi: 10.1111/brv.12302.

Curry, K. A. 1999. Ontogenetic histology of *Apatosaurus* (Dinosauria: Sauropoda): new insights on growth rates and longevity. Journal of Vertebrate Paleontology 19:654–665.

Curry Rogers, K. 2002. Titanosaur tails tell two tales: a second Malagasy titanosaur with saltasaurid affinities. Journal of Vertebrate Paleontology 22(3, Supplement):47A–48A.

Curry Rogers, K. 2005. Titanosauria: a phylogenetic overview; pp. 50–103 in K. Curry Rogers and J. A. Wilson (eds.), The Sauropods: Evolution and Paleobiology. University of California Press, Berkeley, California.

Curry Rogers, K. 2009. The postcranial osteology of *Rapetosaurus krausei* (Sauropoda: Titanosauria) from the Late Cretaceous of Madagascar. Journal of Vertebrate Paleontology 29:1046–1086.

Curry Rogers, K., and C. A. Forster. 2001. The last of the dinosaur titans: a new sauropod from Madagascar. Nature 412:530–534.

Curry Rogers, K., and C. A. Forster. 2004. The skull of *Rapetosaurus krausei* (Sauropoda: Titanosauria) from the Late Cretaceous of Madagascar. Journal of Vertebrate Paleontology 24:121–144.

Curry Rogers, K., and M. Imker. 2007. New data on "Malagasy Taxon B," a titanosaur from the Late Cretaceous of Madagascar. Journal of Vertebrate Paleontology 27(3, Supplement):64A.

Curry Rogers, K., and J. A. Wilson. 2014. *Vahiny deperti*, gen. et sp. nov., a new titanosaur (Dinosauria, Sauropoda) from the Upper Cretaceous Maevarano Formation, Madagascar. Journal of Vertebrate Paleontology 34:606–617.

Curry Rogers, K., M. Whitney, M. D. D'Emic, and B. Bagley. 2016. Precocity in a tiny titanosaur from the Late Cretaceous of Madagascar. Science 352:450–454.

Curry Rogers, K., M. D. D'Emic, R. Rogers, M. Vickaryous, and A. Cagan. 2011. Sauropod dinosaur osteoderms from the Late Cretaceous of Madagascar. Nature Communications 2:564. doi: 10.1038/ncomms1578.

Curtin, A. J., G. R. Zug, and J. R. Spotila. 2009. Longevity and growth strategies of the desert tortoise (*Gopherus agassizii*) in two American deserts. Journal of Arid Environments 73:463–471.

Curtin, A. J., A. A. Macdowell, E. G. Schaible, and V. L. Roth. 2012. Noninvasive histological comparison of bone growth patterns among fossil and extant neonatal elephantids using synchrotron radiation X-ray microtomography. Journal of Vertebrate Paleontology 32:939–955.

de Boef, M., and H. Larsson. 2007. Bone microstructure: quantifying bone vascular orientation. Canadian Journal of Zoology 85:63–70.

de Margerie, E. de. 2002. Laminar bone as an adaptation to torsional loads in flapping flight. Journal of Anatomy 201:521–526.

de Margerie, E. de, J. Cubo, and J. Castanet. 2002. Bone typology and growth rates: testing and quantifying 'Amprino's rule' in the mallard (*Anas platyrhynchos*). Comptes Rendus Biologies 325:221–230.

de Margerie, E. de, J. P. Robin, D. Verrier, J. Cubo, R. Groscolas, and J. Castanet. 2004. Assessing a relationship between bone microstructure and growth rate: a fluorescent labeling study in the king penguin chick (*Aptenodytes patagonicus*). Journal of Experimental Biology 207:869–879.

de Ricqlès, A. J. 1983. Cyclical growth in the long limb bones of a sauropod dinosaur. Acta Palaeontologica Polonica 28:225–232.

de Ricqlès, A. J., J. Castanet, and H. Francillon-Vieillot. 2004. The "message" of bone tissue in paleoherpetology. Italian Journal of Zoology Supplement1:3–12.

D'Emic, M. D., J. A. Wilson, and S. Chatterjee. 2009. The titanosaur (Dinosauria: Sauropoda) osteoderm record: review and first definitive specimen from India. Journal of Vertebrate Paleontology 29:165–177.

Dempster, D. W. 1992. Bone remodeling; pp. 355–380 in F. L. Coe and M. J. Favus (eds.), Disorders of Bone and Mineral Metabolism. Raven Press, New York.

Dodson, P., D. W. Krause, C. A. Forster, S. D. Sampson, and F. Ravoavy. 1998. Titanosaurid (Sauropoda) osteoderms from the Late Cretaceous of Madagascar. Journal of Vertebrate Paleontology 18:563–568.

Enlow, D. H., and S. O. Brown. 1956. A comparative histological study of fossil and recent bone tissues, Part I. Texas Journal of Sciences 8:405–443.

Enlow, D. H., and S. O. Brown. 1957. A comparative histological study of fossil and recent bone tissues, Part II. Texas Journal of Sciences 9:186–214.

Enlow, D. H., and S. O. Brown. 1958. A comparative histological study of fossil and recent bone tissues, Part III. Texas Journal of Sciences 10:187–230.

Erickson, G. M., P. J. Makovicky, P. J. Currie, M. A. Norell, S. A. Yerby, and C. A. Brochu. 2004. Gigantism and comparative life-history parameters of tyrannosaurid dinosaurs. Nature 430:772–775.

Felder, A. A., C. Phillips, H. Cornish, M. Cooke, J. R. Hutchinson, and M. Doube. 2017. Secondary osteons scale allometrically in mammalian humerus and femur. Royal Society Open Science. doi: 10.1098/rsos.170431.

Francillon-Vieillot, H., V. De Buffrénil, J. Castanet, J. Géraudie, F. Meunier, J. Sire, L. Zylberberg, and A. J. de Ricqlès. 1990. Microstructure and mineralization of vertebrate skeletal tissues; pp. 471–530 in J. G. Carter (ed.), Skeletal Biomineralization: Patterns, Processes, and Evolutionary Trends. Van Nostrand Reinhold, New York.

Frylestam, B., and T. Schantz. 1977. Age determination of European hares based on periosteal growth lines. Mammal Review 7:151–154.

Gallina, P. A. 2012. Histología ósea del titanosaurio *Bonitasaura salgadoi* (Dinosauria: Sauropoda) del Cretácico superior de Patagonia. Ameghiniana 49:289–302.

García, R. A., L. Salgado, M. S. Fernández, I. A. Cerda, A. P. Carabajal, A. Otero, R. A. Coria, and L. E. Fiorelli. 2015. Paleobiology of titanosaurs: reproduction, development, histology, pneumaticity, locomotion, and neuroanatomy from the South American fossil record. Ameghiniana 52:29–68.

Ghilardi, A. M., T. Aureliano, R. R. C. Duque, M. A. Fernandes, A. M. F. Barreto, and A. Chinsamy. 2016. A new titanosaur from the Lower Cretaceous of Brazil. Cretaceous Research 67:16e24.

González Riga, B. J. 2003. A new titanosaur (Dinosauria: Sauropoda) from the Upper Cretaceous of Mendoza, Argentina. Ameghiniana 40:155–172.

González Riga, B. J., and K. Curry Rogers. 2006. Osteohistology of the titanosaur *Mendozasaurus* (Dinosauria, Suaropoda): preliminary interpretations; p. 84 in 9° Congreso Argentino de Paleontología y Bioestratigraía (Córdoba), Resúmenes. September 18–22, Universidad Nacional de Córdoba, Argentina. Academia Nacional de Cienicas.

Gorscak, E., and P. M. O'Connor. 2016. Time-calibrated models support congruency between Cretaceous continental rifting and titanosaurian evolutionary history. Biology Letters 12:20151047. doi: 10.1098/rsbl.2015.1047.

Havill, L. M. 2003. Osteon remodeling dynamics in *Macaca mulatta*: normal variation with regard to age, sex, and skeletal maturity. Calcified Tissue International 74:95–102.

Horner, J. R., A. J. de Ricqlès, and K. Padian. 1999. Variation in dinosaur skeletochronology indicators: implications for age assessment and physiology. Paleobiology 25:295–304.

Hutton, J. S. M. 1986. Age determination of living Nile crocodiles from the cortical stratification of bone. Copeia 1986:332–341.

Jowsey, J., and K. A. Johnson. 1972. Juvenile osteoporosis: Bone findings in seven patients. Journal of Pediatrics 81:511–517.

Jha, G. J., M. G. Deo, and V. Ramalingaswami. 1968. Bone growth in protein deficiency: a study in rhesus monkeys. American Journal of Pathology 53:1111–1123.

Klein, N., and P. M. Sander. 2008. Ontogenetic stages in the long bone histology of sauropod dinosaurs. Paleobiology 34:247–263.

Klein, N., P. M. Sander, and V. Suteethorn. 2009. Bone histology and its implications for the life history and growth of the Early Cretaceous titanosaur *Phuwiangosaurus sirindhornae*. Geological Society, London, Special Publications 315:217–228.

Klein, N., P. M. Sander, K. Stein, J. Le Loeuff, J. L. Carballido, and E. Buffetaut. 2012. Modified laminar bone in *Ampelosaurus atacis* and other titanosaurs (Sauropoda): implications for life history and physiology. PLoS ONE 7:e36907. doi: 10.1371/journal.pone.0036907.

Klevezal, G. A. 1996. Recording Structures of Mammals: Determination of Age and Reconstruction of Life History. A. A. Balkema Publishers, Brookfield, Vermont, 274 pp.

Klevezal, G. A., A. V. Kaller Sallas, and S. P. Kirpichev. 1972. Determination of age in birds by layers in the periosteal zone. Zoologicheskii Zhurnal 51:1726–1730.

Köhler, M., and S. Moyà-Solà. 2009. Physiological and life history strategies of a fossil large mammal in a resource-limited environment. Proceedings of the National Academy of Sciences of the United States of America 106:20354–20358.

Köhler, M., N. Marin-Moratalla, X. Jordana, and R. Aanes. 2012. Seasonal bone growth and physiology in endotherms sheds light on dinosaur physiology. Nature 487:358–361.

Krause, D. W., and A. H. Rasoamiaramanana. 2006. Late Cretaceous vertebrates of Madagascar: implications for Gondwanan biogeography; pp. 59–62 in P. M. Barrett and S. E. Evans (eds.), Ninth International Symposium on Mesozoic Terrestrial Ecosystems and Biota. Natural History Museum, London.

Krause, D. W., P. M. O'Connor, K. Curry Rogers, S. D. Sampson, G. A. Buckley, and R. R. Rogers. 2006. Late Cretaceous terrestrial vertebrates from Madagascar: implications for Latin

American biogeography. Annals of the Missouri Botanical Garden 93:178–208.

Krause, D. W., R. R. Rogers, C. A. Forster, J. H. Hartman, G. A. Buckley, and S. D. Sampson. 1999. The Late Cretaceous vertebrate fauna of Madagascar: implications for Gondwanan paleobiogeography. GSA Today 9:1–7.

Krause, D. W., J. J. W. Sertich, R. R. Rogers, S. C. Kast, A. H. Rasoamiaramanana, and G. A. Buckley. 2010. Overview of the discovery, distribution, and geological context of *Simosuchus clarki* (Crocodyliformes: Notosuchia) from the Late Cretaceous of Madagascar; pp. 4–12 in D. W. Krause and N. J. Kley (eds.), *Simosuchus clarki* (Crocodyliformes: Notosuchia) from the Late Cretaceous of Madagascar. Society of Vertebrate Paleontology Memoir 10. Journal of Vertebrate Paleontology 30(6, Supplement).

Lacovara, K. J., M. C. Lamanna, L. M. Ibiricu, J. C. Poole, E. R. Schroeter, P. V. Ullmann, K. K. Voegele, Z. M. Boles, A. M. Carter, E. K. Fowler, V. M. Egerton, A. E. Moyer, C. L. Coughenour, J. P. Schein, J. D. Harris, R. D. Martínez, and F. E. Novas. 2014. A gigantic, exceptionally complete titanosaurian sauropod dinosaur from Southern Patagonia, Argentina. Scientific Reports 4:6196. doi: 10.1038/srep06196.

Lambertz, M., F. Bertozzo, and P. M. Sander. 2018. Bone histological correlates for air sacs and their implications for understanding the origin of the dinosaurian respiratory system. Biology Letters 14:20170514. doi: 10.1098/rsbl.2017.0514.

Lamm, E.-T. 2013. Preparation and sectioning of specimens; pp. 55–160 in K. Padian and E.-T. Lamm (eds.), Bone Histology of Fossil Tetrapods: Advancing Methods, Analysis, and Interpretation. University of California Press, Berkeley, California.

Landry, M. and H. Fleisch. 1964. The influence of immobilisation on bone formation as evaluated by osseous incorporation of tetracyclines. The Journal of Bone and Joint Surgery 46B:764–771.

Lanyon, L. E., and D. G. Baggot. 1976. Mechanical function as an influence on the structure and form of bone. The Journal of Bone and Joint Surgery 58B:436–443.

Lawler, J. P., and R. G. White. 1997. Seasonal changes in metabolic rates in muskoxen following twenty-four hours of starvation. Rangifer 17:135–138.

Lee, A. H., and P. M. O'Connor. 2013. Bone histology confirms determinate growth and small body size in the noasaurid theropod *Masiakasaurus knopfleri.* Journal of Vertebrate Paleontology 33:865–876.

Lehman, T., and H. N. Woodward. 2008. Modeling growth rates for sauropod dinosaurs. Paleobiology 34:264–281.

Lindoso, R. M., T. da Silva Marinho, R. M. Santucci, M. A. Medeiros, and I. de Souza Carvalho. 2013. A titanosaur (Dinosauria: Sauropoda) osteoderm from the Alacântar Formation (Cenomanian), São Luís Basin, Northeastern Brazil. Cretaceous Research 45:43–48.

Lozupone, E., and A. Favia. 1990. The structure of the trabeculae of cancellous bone. 2. Long bones and mastoid. Calcified Tissue International 46:367–372.

Marín-Moratalla, N., J. Cubo, X. Jordana, B. Moncunill-Solé, and M. Köhler. 2014. Correlation of quantitative bone histology data with life history and climate: a phylogenetic approach. Biological Journal of the Linnean Society 112:678–687.

Martin, D. L., and G. J. Armelagos. 1985. Skeletal remodeling and mineralization as indicators of health: an example from prehistoric Sudanese Nubia. Journal of Human Evolution 14:527–537.

Martin, R. 2003. Fatigue damage, remodeling, and the minimization of skeletal weight. Journal of Theoretical Biology 220:271–276.

Martin, R., D. B. Burr, N. A. Sharkey, and D. P. Fyhrie. 2015. Skeletal Tissue Mechanics, second edition. Springer, New York, 501 pp.

Mazzetta, G. V., P. Christiansen, and R. A. Farina. 2004. Giants and bizarres: body size of some southern South American Cretaceous dinosaurs. Historical Biology 2004:1–13.

McCarthy, E. F., and F. J. Frassica. 1998. Pathology of Bone and Joint Disorders with Clinical and Radiographic Correlation. W.B. Saunders Company, Philadelphia, 385 pp.

McFarlin, S. C., C. Terranova, A. L. Zihlman, D. H. Enlow, and T. G. Bromage. 2008. Regional variability in secondary remodeling within long bone cortices of catarrhine primates: the influence of bone growth history. Journal of Anatomy 213:308–324.

McNab, B. K. 2002. The Physiological Ecology of Vertebrates: A View from Energetics. Cornell University Press, Ithaca, New York, 608 pp.

McNulty, K., K. Curry Rogers, and O. Rudloff. 2010. Morphometric analyses of titanosaur caudal vertebrae: implications for naming "Malagasy Taxon B." Journal of Vertebrate Paleontology 30(Program and Abstracts):133A.

Mitchell, J., and P. M. Sander. 2014. The three-front model: a developmental explanation of long bone diaphyseal histology of Sauropoda. Biological Journal of the Linnean Society 112:765–781.

Montes, L., J. Castanet, and J. Cubo. 2010. Relationship between bone growth rate and bone tissue organization in amniotes: first test of Amprino's rule in a phylogenetic context. Animal Biology 60:35–41.

Mori, R., T. Kodaka, S. Soeta, J. Sato, J. Kakino, S. Hamato, H. Takaki, and Y. Naito. 2005. Preliminary study of histological comparison on the growth patterns of long-bone cortex in young calf, pig, and sheep. Journal of Veterinary Medical Science 67:1223–1229.

Mori, S., and D. B. Burr. 1993. Increased intracortical remodeling following fatigue damage. Bone 14:103–109.

Morris, P. 1970. A method for determining absolute age in the hedgehog. Journal of Zoology 161:277–281.

Mundy, G. R. 1987. Bone resorption and turnover in health and disease. Bone 8(1, Supplement):S9–S16.

Nganvongpanit, K., P. Siengdee, K. Buddhachat, J. L. Brown, S. Klinhom, T. Pitakarnnop, T. Angkawanish, and C. Thitaram. 2016. Anatomy, histology, and elemental profile of long bones and ribs of the Asian elephant (*Elephas maximus*). Anatomical Science International. doi: 10.1007/s12565-016-361-y.

Ostrowski, S., P. Mesochina, and J. B. Williams. 2006. Physiological adjustments of Sand Gazelles (*Gazella subgutturosa*) to a boom-or-bust economy: standard fasting metabolic rate, total evaporative water loss, and changes in the sizes of organs during food and water restriction. Physiological and Biochemical Zoology 79:810–819.

Paleobiology Database. 2017. Titanosauria [search parameters: group = Titanosauria, time interval = Cretaceous, region = global]. Available at paleobiodb.org. Accessed June 15, 2017.

Parfitt, A. M. 1987. Bone and plasma calcium homeostasis. Bone 8(1, Supplement):S1–S8.

Pfeiffer, S., C. Crowder, L. Harrington, and M. Brown. 2006. Secondary osteon and Haversian canal dimensions as behavioral indicators. American Journal of Physical Anthropology 131:460–468.

Ponton, F., A. Elzanowski, J. Castanet, A. Chinsamy, E. de Margerie, A. J. de Ricqlès, and J. Cubo. 2004. Variation of the outer circumferential layer in the limb bones of birds. Acta Ornithological 39:21–24.

Powell, J. E. 1992. Hallazgo de huevos asignables a dinosaurios Titanosauridae (Saurischia, Sauropoda) de la Provincia de Río Negro, Argentina. Acta Zoologica Lilloana 41:381–394.

Powell, J. E. 2003. Revision of South American titanosaurid dinosaurs: palaeobiological, palaeobiogeographical, and phylogenetic aspects. Records of the Queen Victoria Museum 111:1–173.

Pratt, C. W. M., and R. A. McCance. 1960. Severe undernutrition in growing and adult animals. British Journal of Nutrition 14:75–84.

Rimblot-Baly, F., A. J. de Ricqlès, and L. Zylberberg. 1995. Analyse paléohistologique d'une série de croissance partielle chez *Lapparentosaurus madagascariensis* (Jurassique moyen): essai sur la dynamique de croissance d'un dinosaur sauropode. Annales de Paléontologie 81:49–86.

Rogers, R. R. 2005. Fine-grained debris flows and extraordinary vertebrate burials in the Late Cretaceous of Madagascar. Geology 33:297–300.

Rogers, R. R., J. H. Hartman, and D. W. Krause. 2000. Stratigraphic analysis of Upper Cretaceous rocks in the Mahajanga Basin, northwestern Madagascar: implications for ancient and modern faunas. Journal of Geology 108:275–301.

Rogers, R. R., D. W. Krause, and K. Curry Rogers. 2003. Cannibalism in the Madagascan dinosaur *Majungatholus atopus*. Nature 422:515–518.

Rogers, R. R., D. W. Krause, K. Curry Rogers, A. Rasoamiaramanana, and L. Rahantarisoa. 2007. Paleoenvironment and paleoecology

of *Majungasaurus crenatissimus* (Theropoda: Abelisauridae) from the Late Cretaceous of Madagascar; pp. 21–31 in S. D. Sampson and D. W. Krause (eds.), *Majungasaurus crenatissimus* (Theropoda: Abelisauridae) from the Late Cretaceous of Madagascar. Society of Vertebrate Paleontology Memoir 8. Journal of Vertebrate Paleontology 27(2, Supplement).

Salgado, L. 2013. Considerations on the bony plates assigned to titanosaurs. Ameghiniana 40:441–456.

Salgado, L., and R. A. Coria. 2005. Sauropods of Patagonia: systematic update and notes on global sauropod evolution; pp. 430–453 in V. Tidwell and K. Carpenter (eds.), Thunder-lizards: The Sauropodomorph Dinosaurs. Indiana University Press, Bloomington and Indianapolis, Indiana.

Salgado, L., S. Apesteguía, and S. E. Heredia. 2005. A new specimen of *Neuquensaurus australis*, a Late Cretaceous saltasaurine titanosaur from North Patagonia. Journal of Vertebrate Paleontology 25:623–634.

Sampson, S. D., and D. W. Krause. 2007. *Majungasaurus crenatissimus* (Theropoda: Abelisauridae) from the Late Cretaceous of Madagascar. Society of Vertebrate Paleontology Memoir 8. Journal of Vertebrate Paleontology 27(2, Supplement).

Sampson, S. D., M. T. Carrano, and C. A. Forster. 2001. A bizarre predatory dinosaur from the Late Cretaceous of Madagascar. Nature 409:504–506.

Sander, P. M. 2000. Long bone histology of the Tendaguru sauropods: implications for growth and biology. Paleobiology 26:466–488.

Sander, P. M., and P. Andrassy. 2006. Lines of arrested growth and long bone histology in Pleistocene large mammals from Germany: what do they tell us about dinosaur physiology? Palaeontographica A 277:143–159.

Sander, P. M., and M. Clauss. 2008. Sauropod gigantism. Science 322:200–201.

Sander, P. M., and N. Klein. 2005. Developmental plasticity in the life history of a prosauropod dinosaur. Science 310:1800–1802.

Sander, P. M., and C. Tückmantel. 2003. Bone lamina thickness, bone apposition rates, and age estimates in sauropod humeri and femora. Paläontologische Zeitschrift 77:161–172.

Sander, P. M., N. Klein, K. Stein, and O. Wings. 2011. Sauropod bone histology and implications for sauropod biology; pp. 276–302 in N. Klein, K. Remes, C. T. Gee, and P. M. Sander (eds.), Biology of the Sauropod Dinosaurs: Understanding the Life of Giants. Indiana University Press, Bloomington, Indiana.

Sander, P. M., O. Mateus, T. Laven, and N. Knötschke. 2006. Bone histology indicates insular dwarfism in a new Late Jurassic sauropod dinosaur. Nature 441:739–741.

Sander, P. M., N. Klein, E. Buffetaut, G. Cuny, V. Suteethorn, and J. Le Loueff. 2004. Adaptive radiation in sauropod dinosaurs: bone histology indicates rapid evolution of giant body size through acceleration. Organisms Diversity and Evolution 4:165–173.

Schock, C. C., F. R. Noyes, M. M. Crouch, and C. H. E. Matthews. 1975. The effects of immobility on long bone remodeling in the rhesus monkey. Ford Hospital Medical Journal 23:107–115.

Skedros, J. G., K. E. Keenan, T. J. Williams, and C. J. Kiser. 2013. Secondary osteon size and collagen/lamellar organization ("osteon morphotypes") are not coupled, but potentially adapt independently for local strain mode or magnitude. Journal of Structural Biology 181:95–107.

Smith, R. 1994. Idiopathic osteoporosis in the young. Journal of Bone and Joint Surgery 62B:417–428.

Starck, J. M., and A. Chinsamy. 2002. Bone microstructure and developmental plasticity in birds and other dinosaurs. Journal of Morphology 254:232–246.

Stein, K., and P. M. Sander. 2009. Histological core drilling: a less destructive method for studying bone histology; pp. 69–80 in M. A. Brown, J. F. Kane, and W. G. Parker (eds.), Methods in Fossil Preparation: Proceedings of the First Annual Fossil Preparation and Collections Symposium. Petrified Forest, Arizona.

Stein, K., Z. Csiki, K. Curry Rogers, D. B. Weishampel, R. Redelstorff, J. Carballido, and P. M. Sander. 2010. Small body size and extreme cortical remodeling indicate phyletic dwarfism in *Magyarosaurus dacus* (Sauropoda:Titanosauria). Proceedings of the National Academy of Sciences of the United States of America 107:9258–9263.

Stover, S. M., R. R. Pool, R. B. Martin, and J. P. Morgan. 1992. Histological features of the dorsal cortex of the third metacarpal bone mid-diaphysis during postnatal growth in thoroughbred horses. Journal of Anatomy 181:455–469.

Straehl, F. R., T. M. Scheyer, A. M. Forasiepi, R. D. MacPhee, and M. R. Sánchez-Villagra. 2013. Evolutionary patterns of bone histology and bone compactness in xenarthran mammal long bones. PLoS ONE 8:e69275. doi: 10.1371/journal.pone.0069275.

Turvey, S. T., O. R. Green, and R. N. Holdaway. 2005. Cortical growth marks reveal extended juvenile development in New Zealand moa. Nature 435:940–943.

Upchurch, P., P. M. Barrett, and P. Dodson. 2004. Sauropoda; pp. 259–322 in D. B. Weishampel, P. Dodson, and H. Osmólska (eds.), The Dinosauria, second edition. University of California Press, Berkeley, California.

Van Oers, R. F. M., R. Ruimerman, B. van Rietbergen, P. A. J. Hilbers, and R. Huiskes. 2008. Relating osteon diameter to strain. Bone 43:476–482.

Vidal, D., F. Ortega, and J. Sanz. 2014. Titanosaur osteoderms from the Upper Cretaceous of Lo Hueco (Spain) and their implications on the armor of Laurasian titanosaurs. PLoS ONE 9:e102488. doi: 10.1371/journal.pone.0102488.

Vidal, D., F. Ortega, F. Gascó, A. Serrano-Martínez, and J. L. Sanz. 2017. The internal anatomy of titanosaur osteoderms from the Upper Cretaceous of Spain is compatible with a role in oogenesis. Scientific Reports 7:42035. doi: 10.1038/srep42035.

Weinreb, M., G. A. Rodan, and D. D. Thompson. 1989. Osteopenia in the immobilized rat hind limb is associated with increased bone resorption and decreased bone formation. Bone 10:187–194.

Wilson, J. A. 2002. Sauropod dinosaur phylogeny: critique and cladistic analysis. Zoological Journal of the Linnean Society 136:217–276.

Wilson, J. A. 2005a. Overview of sauropod phylogeny and evolution; pp. 15–49 in K. Curry Rogers and J. A. Wilson (eds.), The Sauropods: Evolution and Paleobiology. University of California Press, Berkeley, California.

Wilson, J. A. 2005b. Redescription of the Mongolian sauropod *Nemegtosaurus mongoliensis* Nowinski (Dinosauria: Saurischia) and comments on Late Cretaceous sauropod diversity. Journal of Systematic Palaeontology 3:283–318.

Wilson, J. A., and M. T. Carrano. 1999. Titanosaur locomotion and the origin of "wide-gauge" trackways: a biomechanical and systematic perspective on sauropod locomotion. Paleobiology 25:252–267.

Wilson, J. A., and P. Upchurch. 2003. A revision of *Titanosaurus* (Dinosauria - Sauropoda), the first 'Gondwanan' dinosaur genus. Journal of Systematic Palaeontology 1:125–160.

Wilson, J. A., D. Pol, A. B. Carvalho, and H. Zaher. 2016. The skull of the titanosaur *Tapuiasaurus macedoi* (Dinosauria: Sauropoda), a basal titanosaur from the Lower Cretaceous of Brazil. Zoological Journal of the Linnean Society 178:611–662. doi: 10.1111/zoj.12420.

Woodward, H. N., and T. M. Lehman. 2009. Bone histology and microanatomy of *Alamosaurus sanjuanensis* (Sauropoda: Titanosauria) from the Maastrichtian of Big Bend National Park, Texas. Journal of Vertebrate Paleontology 29:807–821.

Woodward, H. N., J. R. Horner, and J. O. Farlow. 2011. Osteohistological evidence for determinate growth in the American alligator. Journal of Herpetology 45:339–342.

Woodward, H., K. Padian, and A. Lee. 2013. Skeletochronology; pp. 187–207 in K. Padian and E.-T. Lamm (eds.), Bone Histology of Fossil Tetrapods: Advancing Methods, Analysis, and Interpretation. University of California Press, Berkeley, California.

Woodward, H. N., E. A. F. Fowler, J. O. Farlow, and J. R. Horner. 2015. *Maiasaura*, a model organism for extinct vertebrate population biology: a large sample statistical assessment of growth dynamics and survivorship. Paleobiology 41:503–527.

Wronski, T. M., and E. R. Morey. 1983. Inhibition of cortical and trabecular bone formation in the long bones of immobilized monkeys. Clinical Orthopaedics 181:269–276.

Young, D. R., and V. S. Schneider. 1981. Radiographic evidence of disuse osteoporosis in the monkey (*M. nemestrina*). Calcified Tissue International 33:631–639.

Young, D. R., W. J. Niklowitz, and C. R. Steele. 1983. Tibial changes in experimental disuse osteoporosis in the monkey. Calcified Tissue International 35:304–308.

Young, D. R., W. H. Howard, C. Cann, and C. R. Steele. 1979. Noninvasive measure of bone bending rigidity in the monkey (*M. nemestrina*). Calcified Tissue International 27:109–115.

Young, D. R., W. J. Niklowitz, R. J. Brown, and W. S. S. Jee. 1986. Immobilization-associated osteoporosis in primates. Bone 7:109–117.

Zedda, M., G. Lepore, P. Manca, V. Chisu, and V. Farina. 2008. Comparative bone histology of adult horses (*Equus caballus*) and cows (*Bos taurus*). Anatomia, Histologia, Embryologica 37:442–445.

Zurriaguz, V. 2017. New record of titanosaurian (Dinosauria: Sauropodomorpha) osteoderms from the Upper Cretaceous of North Patagonia. Cretaceous Research 74:175–180.

Submitted July 26, 2017; revisions received May 11, 2018; accepted May 12, 2018.
Handling editor: Michael D'Emic.